

The *XMM-Newton* Serendipitous Survey

V. Optical identification of the *XMM-Newton* Medium sensitivity Survey (XMS)[★]

X. Barcons¹, F.J. Carrera¹, M.T. Ceballos¹, M.J. Page², J. Bussons-Gordo¹, A. Corral¹, J. Ebrero¹, S. Mateos^{1,3}, J.A. Tedds³, M.G. Watson³, D. Baskill³, M. Birkinshaw⁴, T. Boller⁵, N. Borisov⁶, M. Bremer⁴, G.E. Bromage⁷, H. Brunner⁵, A. Caccianiga⁸, C.S. Crawford⁹, M.S. Cropper², R. Della Ceca⁸, P. Derry³, A.C. Fabian⁹, P. Guillout¹⁰, Y. Hashimoto⁵, G. Hasinger⁵, B.J.M. Hassall⁷, G. Lamer¹¹, N.S. Loaring^{2,12}, T. Maccacaro⁸, K.O. Mason², R.G. McMahon⁹, L. Mirioni¹⁰, J.P.D. Mittaz², C. Motch¹⁰, I. Negueruela^{10,13}, J.P. Osborne³, F. Panessa¹, I. Pérez-Fournon¹⁴, J.P. Pye³, T.P. Roberts^{3,15}, S. Rosen^{2,3}, N. Schartel¹⁶, N. Schurch^{3,15}, A. Schwone¹¹, P. Severgnini⁸, R. Sharp^{9,17}, G.C. Stewart³, G. Szokoly⁵, A. Ullán^{1,18}, M.J. Ward^{3,15}, R.S. Warwick³, P.J. Wheatley^{3,19}, N.A. Webb²⁰, D. Worrall⁴, W. Yuan^{9,21}, and H. Ziaeepour²

¹ Instituto de Física de Cantabria (CSIC-UC), 39005 Santander, Spain

² Mullard Space Science Laboratory, University College London, Holmbury St. Mary, Dorking, Surrey RH5 6NT, UK

³ X-ray and Observational Astronomy Group, Department of Physics and Astronomy, Leicester University, Leicester LE1 7RH, UK

⁴ H.H. Wills Physics Laboratory, University of Bristol, Tyndall Avenue, Bristol BS8 1TL, UK

⁵ Max-Planck-Institut für Extraterrestrische Physik, Giessenbachstrasse, 85740 Garching, Germany

⁶ Special Astrophysical Observatory, 369167 Nizhniy Arkhyz, Russia

⁷ Centre for Astrophysics, University of Central Lancashire, Preston PR1 2HE, UK

⁸ INAF - Osservatorio Astronomico di Brera, via Brera 28, 20121 Milano, Italy

⁹ Institute of Astronomy, Madingley Road, Cambridge CB3 0HA, UK

¹⁰ Observatoire Astronomique de Strasbourg, 11 rue de l'Université, 67000 Strasbourg, France

¹¹ Astrophysikalisches Institut Potsdam, An der Sternwarte 16, 144482, Potsdam, Germany

¹² South African Large Telescope, P.O. Box 9, Observatory, 7935, South Africa

¹³ Departamento de Física, Ingeniería de Sistemas y Teoría de la Señal, Universidad de Alicante, 03080 Alicante, Spain

¹⁴ Instituto de Astrofísica de Canarias, 38200 La Laguna, Spain

¹⁵ Department of Physics, University of Durham, South Road, Durham DH1 3LE, UK

¹⁶ European Space Astronomy Centre, Apartado 50727, 28080 Madrid, Spain

¹⁷ Anglo-Australian Observatory, PO Box 296, Epping, NSW 1710, Australia

¹⁸ Centro de Astrobiología (CSIC-INTA), P.O. Box 50727, 28080 Madrid, Spain

¹⁹ Department of Physics, University of Warwick, Coventry CV4 7AL, UK

²⁰ Centre d'Etude Spatiale des Rayonnements, CNRS/UPS, 9 Avenue du Colonel Roche, 31028 Toulouse Cedex 04, France

²¹ National Astronomical Observatories of China/Yunnan Observatory, Phoenix Hill, PO Box 110, Kunming, Yunnan, China

Received 30 May 2007; accepted 2007

ABSTRACT

Aims. X-ray sources at intermediate fluxes (a few $\times 10^{-14}$ erg cm $^{-2}$ s $^{-1}$) with sky density of ~ 100 deg $^{-2}$, are responsible for a significant fraction of the cosmic X-ray background at various energies below 10 keV. The aim of this paper is to provide an unbiased and quantitative description of the X-ray source population at these fluxes and in various X-ray energy bands.

Methods. We present the *XMM-Newton* Medium sensitivity Survey (XMS), including a total of 318 X-ray sources found among the serendipitous content of 25 *XMM-Newton* target fields. The XMS comprises four largely overlapping source samples selected at soft (0.5–2 keV), intermediate (0.5–4.5 keV), hard (2–10 keV) and ultra-hard (4.5–7.5 keV) bands, the first three of them being flux-limited.

Results. We report on the optical identification of the XMS samples, complete to 85–95%. At the flux levels sampled by the XMS we find that the X-ray sky is largely dominated by Active Galactic Nuclei. The fraction of stars in soft X-ray selected samples is below 10%, and only a few per cent for hard selected samples. We find that the fraction of optically obscured objects in the AGN population stays constant at around 15–20% for soft and intermediate band selected X-ray sources, over 2 decades of flux. The fraction of obscured objects amongst the AGN population is larger (~ 35 –45%) in the hard or ultra-hard selected samples, and constant across a similarly wide flux range. The distribution in X-ray-to-optical flux ratio is a strong function of the selection band, with a larger fraction of sources with high values in hard selected samples. Sources with X-ray-to-optical flux ratios in excess of 10 are dominated by obscured AGN, but with a significant contribution from unobscured AGN.

Key words. X-rays: general, galaxies, stars; Galaxies: active

Send offprint requests to: X. Barcons

* Based on observations obtained with *XMM-Newton*, an ESA science mission with instruments and contributions directly funded by

ESA Member States and the USA (NASA). Based on observations made with the INT/WHT, TNG and NOT operated on the island of La Palma by the Isaac Newton Group, the Centro Galileo Galilei and

1. Introduction

Supermassive black holes (SMBHs, i.e., with masses $\sim 10^6 - 10^9 M_\odot$) have been detected in the centers of virtually all nearby galaxies (Merritt & Ferrarese, 2001; Tremaine et al., 2002). In many of these galaxies -including our own-, the SMBH is largely dormant, i.e., the luminosity is many orders of magnitude below the Eddington limit. Only $\sim 10\%$ of today's galaxies (at most) host active galactic nuclei (AGN), and a very large fraction of them are in fact inconspicuous at most wavelengths because of obscuration (Fabian & Iwasawa, 1999).

It is generally believed that the seeds of these SMBHs were the remnants of the first generation of massive stars in the history of the Universe. These early black holes may have had masses of tens of M_\odot at most. The growth of these relic black holes to their current sizes is very likely dominated by accretion, with additional contributions by other phenomena like black hole mergers and tidal capture of stars (Marconi et al., 2004). According to current synthesis models, the integrated X-ray emission produced by the growth of SMBHs by accretion over the history of the Universe is recorded in the X-ray background (XRB). Thus the XRB can be used to constrain the epochs and environments in which SMBHs developed.

There are currently a number of existing or on-going surveys in various X-ray energy bands (see Brandt & Hasinger (2005) for a recent compilation). In the pre-Chandra and pre-*XMM-Newton* era the Einstein Extended Medium Sensitivity Survey (Maccacaro et al., 1982; Gioia et al., 1990; Stocke et al., 1991) pioneered the procedure of determining typical X-ray to optical flux ratios for different classes of X-ray sources to facilitate the identification processes and has set the standards for serendipitous X-ray surveys. *ROSAT* produced a number of surveys in the soft 0.5-2 keV X-ray band at various depths, e.g., the *ROSAT* Bright Survey (Schwope et al., 2000), the intermediate flux RIXOS survey (Mason et al., 2000) and the *ROSAT* deep surveys (McHardy et al., 1998; Georgantopoulos et al., 1996; Hasinger et al., 1998; Lehmann et al., 2001) among others. These surveys show that AGN dominate the high Galactic latitude soft X-ray sky at virtually all relevant fluxes. The majority of these AGN are of spectroscopic type 1, which means that we are witnessing the growth of SMBH through unobscured lines of sight. In a moderate fraction of the sources identified, however, there is evidence for obscuration as their optical spectra lack broad emission lines (type 2 AGN).

Ueda et al. (2003) discuss the results from a large area X-ray survey in the 2-10 keV band with ASCA and those from HEAO-1 and *Chandra*, where a larger fraction of the sources identified correspond to type 2 AGN.

With *Chandra* and *XMM-Newton* coming into operation X-ray surveys, particularly at energies above a few keV, have been significantly boosted. Thanks to the high sensitivity and large field of view of the EPIC cameras (Turner et al., 2001; Strüder et al., 2001) on board *XMM-Newton* (Jansen et al., 2001), X-ray surveys requiring large solid angles have been dominated by this instrument. The Bright Source Survey-BSS (Della Ceca et al., 2004) contains 400 sources brighter than $\sim 7 \times 10^{-14} \text{ erg cm}^{-2} \text{ s}^{-1}$ either in 0.5-4.5 keV or 4.5-7.5 keV.

the Nordic Optical Telescope Science Association respectively, in the Spanish Observatorio del Roque de los Muchachos. Based on observations collected at the Centro Astronómico Hispano Alemán (CAHA) at Calar Alto, operated jointly by the Max-Planck Institut für Astronomie and the Instituto de Astrofísica de Andalucía (CSIC). Based on observations collected at the European Southern Observatory, Paranal, Chile, as part of programme 75.A-0336

The BSS samples¹, which have been identified to $\sim 90\%$ (Caccianiga et al., 2007), show an X-ray sky dominated by AGN, where the fraction of obscured objects varies with the selection band (sample selection at harder energies reveals a higher fraction of obscured objects as expected).

Deep surveys have also been conducted by *XMM-Newton*, for example in the Lockman Hole down to $\sim 10^{-15} \text{ erg cm}^{-2} \text{ s}^{-1}$ (Hasinger et al., 2001; Mateos et al., 2005b). However, thanks to its much better angular resolution, the *Chandra* deep surveys are photon counting limited and far from confusion and are consequently much more competitive at fainter fluxes (Alexander et al., 2003; Tozzi et al., 2006). Optical identification of these deep surveys is largely incomplete, a fact that is driven by the intrinsic faintness and red colour of most of the counterparts to the faintest X-ray sources. In the intermediate flux regime, however, the identified fractions are large and nearing completion. It is interesting to note that deep surveys start to find a population of galaxies not necessarily hosting active nuclei as an important ingredient. In addition, the AGN population is found to contain an important fraction of obscured objects.

The wide range of intermediate X-ray fluxes, between say $10^{-15} \text{ erg cm}^{-2} \text{ s}^{-1}$ and $10^{-13} \text{ erg cm}^{-2} \text{ s}^{-1}$ have also been the subject of a number of on-going surveys. Besides bridging the gap between wide and deep surveys, intermediate fluxes sample the region around the break in the X-ray source counts (Carrera et al., 2007), and therefore their sources are responsible for a large fraction of the X-ray background. Among these, we highlight the *XMM-Newton* survey in the well-studied (at many bands) COSMOS field, which covers 2 deg² to fluxes $\sim 10^{-15} \text{ erg cm}^{-2} \text{ s}^{-1}$ (Hasinger et al., 2007). The optical identification is still on-going, reaching 40% (Brusa et al., 2007). At fluxes around $10^{-14} \text{ erg cm}^{-2} \text{ s}^{-1}$, the HELLAS2XMM survey (Baldi et al., 2002; Fiore et al., 2003), now extended to cover 1.4 deg², contains over 220 X-ray sources, optically identified to 70% completeness (Cocchia et al., 2007).

Other surveys in this flux range include the *XMM-Newton* survey in the Marano field (Krumpe et al., 2007), which is 65% identified over a modest solid angle of 0.28 deg². Also the XMM-2dF survey (Tedd et al., in preparation), which contains almost 1000 X-ray sources optically identified in the Southern Hemisphere, is an important contributor in this regime. *Chandra* has also triggered surveys at intermediate fluxes, most notably the *Chandra* Multiwavelength Survey (Kim, D.-W. et al., 2004a,b; Green et al., 2004), covering 1.7 deg² and identified to $\sim 40\%$ completeness (Silverman et al., 2005).

In the realm of this variety of X-ray surveys that yield a qualitative picture of the X-ray sky, the *XMM-Newton* Medium sensitivity Survey (XMS) discussed in this paper, finds its role in three important ways: a) it deals with very large samples, selected at various X-ray bands where *XMM-Newton* is sensitive, from 0.5 to 10 keV; b) the samples that we consider have been identified almost in full, from 85% to 95% completeness and c) three out of the four samples that we explore are strictly flux limited in three energy bands (0.5-2 keV, 0.5-4.5 keV and 2-10 keV). Armed with these unique features, the XMS is a very powerful tool to derive a *quantitative* characterization of the population of X-ray sources selected in various bands, and also to study and characterize minority populations, all of it at specific intermediate X-ray fluxes where a substantial fraction of the X-ray background below 10 keV is generated. The power of the XMS is enhanced by the fact that to some extent it is a represen-

¹ <http://www.brera.mi.astro.it/~xmm/>

tative sub-sample of the *XMM-Newton* X-ray source catalogue 2XMM², containing 150,000 entries.

Specific goals that have driven the construction of the XMS whose results are presented in this paper include: a) quantify the fraction of stars versus extragalactic sources at intermediate X-ray fluxes and at different X-ray energy bands; b) quantify the fraction of AGN that are classified as obscured by optical spectroscopy at intermediate X-ray fluxes and for samples selected in different energy bands; c) find the redshift distribution for the various classes of extragalactic sources and compare soft and hard X-ray selected samples; d) study the distribution of the X-ray-to-optical flux ratio for the various classes of X-ray sources, also as a function of X-ray selection band. The X-ray spectral properties of the sources of the XMS were already discussed in Mateos et al. (2005a).

Further goals that we will achieve with the XMS in forthcoming papers include: e) determine the fraction of “red QSOs” at intermediate X-ray fluxes and as a function of X-ray selection band; f) relate X-ray spectral properties (like photoelectric absorption) to optical colours of the counterpart; g) quantify the fraction of radio-loud AGN in the samples selected at various X-ray energies; h) construct Spectral Energy Distributions for the various classes of sources in the XMS. Results on these further aspects will be presented in a forthcoming paper (Bussoms-Gordo et al., in preparation).

The paper is organized as follows: in Section 2 we define the XMS along with the 4 samples that constitute it, including the X-ray source list; in Section 3 we discuss the multi-band optical imaging conducted on the *XMM-Newton* target fields and the process for selecting candidate counterparts; this is continued in Section 4 where we discuss the identification of the XMS sources in terms of optical spectroscopy, and list photometric and spectroscopic information on each XMS source. Section 5 presents the first scientific results from the XMS, specifically a description of the overall source populations, the fraction of stars in the various samples, the fraction of optically obscured AGN, and the X-ray to optical flux ratio of the different source populations. Section 6 summarizes our main results.

To clarify the terminology used in this paper, an AGN not displaying broad emission lines in its optical spectrum is termed as type 2 or obscured, and type 1 or unobscured otherwise. The property of being absorbed or unabsorbed refers only to the detection or not of photoelectric X-ray absorption. Throughout this paper, we used a single power law X-ray spectrum to convert from X-ray source count rate to flux in physical units, with a photon spectral index $\Gamma = 1.8$ for the XMS-S and XMS-X samples and $\Gamma = 1.7$ for the XMS-H and XMS-U samples. These are the average values obtained by Carrera et al. (2007), which -as opposed to what we do here- used the specific value of Γ for each individual source and energy range. When computing luminosities, we also use the above spectra for K-correction and the concordance cosmology parameter values: $H_0 = 70 \text{ km s}^{-1} \text{ Mpc}^{-1}$, $\Omega_m = 0.3$ and $\Omega_\Lambda = 0.7$. All quoted uncertainties in parameter estimates are shown at 90% confidence level for one interesting parameter.

2. The *XMM-Newton* Medium sensitivity Survey (XMS)

The XMS is a serendipitous X-ray source survey with intermediate X-ray fluxes, which has been built using the AXIS³ sample described in Carrera et al. (2007). The XMS uses 25 target fields (see table 2, areas around targets themselves are excluded), which cover a geometric sky area $\sim 3 \text{ deg}^2$. The details of the source searching, screening, masking out of problematic detector areas (CCD gaps, bright targets, bad pixels and columns and out of time events) are extensively discussed in Carrera et al. (2007).

The XMS itself is made of four largely overlapping samples. The XMS-S, XMS-H and XMS-X are flux limited in the 0.5-2 keV, 2-10 keV and 0.5-4.5 keV bands respectively, with flux limits, well above the sensitivity of the data, listed in Table 3. A fourth sample (XMS-U) selected in the “ultrahard” band 4.5-7.5 keV is not artificially limited in flux, and due to the scarcity of these sources it contains all the sources detected in the 25 fields. Table 2 lists the X-ray source positions and fluxes in the various bands.

The XMS-S and XMS-H were constructed to match the standard “soft” and “hard” X-ray bands that have been extensively used in previous and contemporary X-ray surveys with *XMM-Newton* and other X-ray observatories. The 0.5-4.5 keV selection band of the XMS-X sample was chosen to maximize the *XMM-Newton*/EPIC sensitivity and indeed is the largest of the 4 samples. The total number of distinct X-ray sources in the XMS is 318, out of which 272 (86%) have been spectroscopically identified. The identification completeness of the various samples is also shown in Table 3, which exceeds 90% for the softer XMS-S and XMS-X samples, and is around 85% for the hard XMS-H and ultra-hard XMS-U samples. The XMS-X sample extends by an order of magnitude the size of the pilot study presented in Barcons et al. (2002).

3. Imaging and selection of candidate counterparts

3.1. The data

Target fields were observed primarily with the Wide-Field Camera (WFC) on the 2.5m INT telescope. The observations were obtained via the AXIS programme and other programmes devoted to image a large number of *XMM-Newton* target fields in the optical. The WFC covers virtually all the field of view of EPIC, if centered optimally. We used the Sloan Digital Sky Survey filters g' , r' and i' to image all the XMS target fields. In addition many of the fields were also imaged bluewards and redwards using existing facility filters at the WFC (u and Z Gunn). These data are available for all fields, except for the G 133-69 pos 1 and PB 5062 fields, while for UZ Lib and B2 1128+31 the u -band data are missing. Since data from these two additional filters are not used in this paper, we do not discuss them any further.

Exposure times were adjusted to be deep enough for most of the X-ray sources to have an optical counterpart in the r' and i' filters, and therefore had to be significantly deeper than those in the Digitized Sky Surveys. They were chosen as 600s, 600s and 1200s respectively in the g' , r' , i' filters for dark time. This

² Pre-release under <http://xmm.vilspa.esa.es/xsa>

³ AXIS (An *XMM-Newton* International Survey) was an International Time Programme of the Observatorio del Roque de Los Muchachos, which was granted observing time in years 2000 and 2001. See <http://venus.ifca.unican.es/~xray/AXIS> for details

Table 1. XMS target fields

Target Field	RA (J2000)	DEC (J2000)	b'' (deg)	Phot ^a
Cl 0016+1609	00:18:33	+16:26:18	-45.5	SDSS
G 133-69 pos2	01:04:00	-06:42:00	-69.3	CMC
G 133-69 pos1	01:04:24	-06:24:00	-68.7	CMC
SDS-1b	02:18:00	-05:00:00	-59.7	CMC
SDS-3	02:18:48	-04:39:00	-59.3	CMC
SDS-2	02:19:36	-05:00:00	-58.9	CMC
A 399	02:58:25	+13:18:00	-39.2	CMC
Mrk 3	06:15:36	+71:02:05	+22.7	WFC ^b
MS 0737.9+7441	07:44:04	+74:33:49	+29.6	WFC
S5 0836+71	08:41:24	+70:53:41	+34.4	WFC
Cl 0939+4713	09:43:00	+46:59:30	+48.9	SDSS
B2 1028+31	10:30:59	+31:02:56	+59.8	SDSS
B2 1128+31	11:31:09	+31:14:07	+72.0	SDSS
Mrk 205	12:21:44	+75:18:37	+41.7	WFC
MS 1229.2+6430	12:31:32	+64:14:21	+53.0	SDSS
HD 117555	13:30:47	+24:13:58	+80.7	SDSS
A 1837	14:01:35	-11:07:37	+47.6	CMC
UZ Lib	15:32:23	-08:32:05	+36.6	WFC ^c
PKS 2126-15	21:29:12	-15:38:41	-42.4	CMC
PKS 2135-14	21:37:45	-14:32:55	-43.8	CMC
PB 5062	22:05:10	-01:55:18	-43.3	CMC
LBQS 2212-1759	22:15:32	-17:44:05	-52.9	CMC
PHL 5200	22:28:30	-05:18:55	-50.0	CMC
IRAS 22491-1808	22:51:50	-17:52:23	-61.4	CMC
EQ Peg	23:31:50	+19:56:17	-39.1	CMC

^a This column states what is the ultimate photometric calibration used: WFC if our own data from a photometric night was used as the ultimate resource, SDSS for the Sloan Digital Sky Survey, and CMC for the Carlsberg Meridian Catalogue survey.

^b In this case the extinction curve calibration in our data gives some scatter which means that the magnitudes are not as accurate as for the sources in the other fields.

^c This field was not imaged in g' and r' . In addition to i' , it was imaged in the Johnson filters B, V and R at the ESO/MPG 2.2m telescope with the WFI camera.

Table 3. Summary of identifications in the various samples

Sample	Sel. band (keV)	Limiting flux ^a	Number sources	Number ident.	Fract. (%)
XMS-S	0.5-2.0	1.5	210	200	95
XMS-X	0.5-4.5	2.0	284	261	92
XMS-H	2.0-10	3.3	159	132	83
XMS-U	4.5-7.5	1.15	70	60	86

^a in units of 10^{-14} erg cm $^{-2}$ s $^{-1}$ in the selection X-ray band

produced images with limiting magnitude for point sources going down to $r' \sim 23 - 24$ for $\sim 1 - 1.5''$ seeing, most typical in our observing runs, which experience with the first fields (Barcons et al., 2002) demonstrated to be appropriate. When observing with brighter moon conditions, we restricted ourselves to the reddest filters and doubled the exposure times.

The WFC images were reduced using standard techniques including de-bias, non-linearity correction, flat fielding and fringe correction (in i' and Z). Bias frames and twilight flats obtained during the same observing nights were used, but for the fringe correction, contemporaneous archival i' and Z fringe frames were utilised. Information on the WFC pipeline procedures, which performs all these steps can be found under the Cambridge Astronomy Survey Unit⁴ (CASU) web pages.

3.2. Photometric calibration

The photometric calibration of the WFC images was conducted in the standard way. Photometric standard stars were observed during the same nights as the *XMM-Newton* target fields were imaged, at different air masses. Then an extinction curve was fitted for each optical band. In several cases were we suspected that photometric conditions were not fulfilled by the original data, we re-imaged the same field with one WFC filter (r') or alternatively a part of it with the ALFOSC instrument in imaging mode on the NOT telescope.

However, in a number of target fields and for some of the bands, the extinction curve showed significant scatter that was attributed to these observations being done under non-photometric conditions. In order to improve the photometric quality of the data, two steps were taken. First we concentrated on calibrating one band (typically r') and later we applied colour corrections to propagate the improved photometry to all bands.

In the first step we used two complementary data sets photometrically calibrated. The first of these is the Sloan Digital Sky Survey, Data Release 5⁵. We could use the SDSS data on 6 *XMM-Newton* fields. The sky density of SDSS is indeed lower than our WFC images, but still we found typically a large enough number (~ 100) of matches in every image.

The second data set used to improve the photometric calibration is the Carlsberg Meridian Catalogue (CMC) astrometric survey in the r' band⁶, which we could apply to 19 fields.

⁵ <http://www.sdss.org>

⁶ see <http://www.ast.cam.ac.uk/~dwe/SRF/camc.html> for details

⁴ <http://www.ast.cam.ac.uk/~wfcsur>

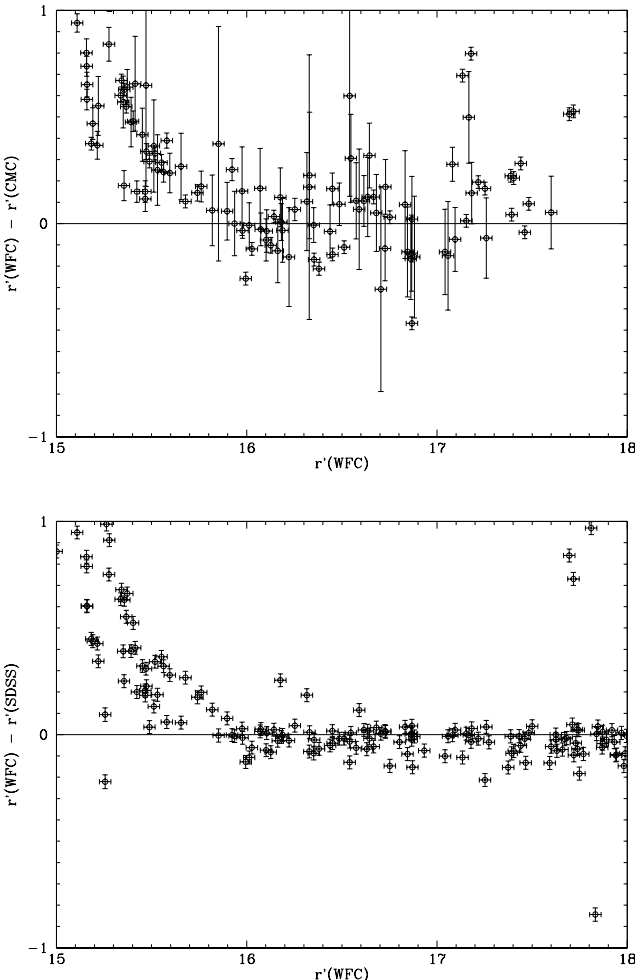


Fig. 1. Photometric cross-calibration in the B2 1128+31 field, where we have both coverage from the SDSS and CMC, along with our own WFC photometry.

This survey is indeed much shallower than the SDSS ($r' < 17$). In addition we found very significant systematic differences between WFC magnitudes and CMC ones at magnitudes smaller than $r' \sim 16 - 16.5$ which we attributed to saturation in our data. That typically leaves a very narrow dynamic range for cross-calibrating WFC versus CMC magnitudes, that we adopted as $16.5 < r' < 17$. Prompted by this, we also restricted the WFC versus SDSS cross calibration to magnitudes brighter than $r' \sim 16$. As a safety test, we cross-calibrated CMC versus SDSS r' magnitudes in the 5 fields where we could do that, but in this case using the full magnitude range from $r' \sim 14 - 18$ and found tiny significant shifts, all of them well below 0.1 mag in all fields. Fig. 1 illustrates the residuals of the cross-calibration in the case of one target field where we had all three WFC, SDSS and CMC data.

In general, photometric shifts in fields where the quality of the WFC photometric calibration was thought to be good, were found to be small (always $\Delta r' < 0.2$ mag) when calibrated against CMC or SDSS. In other cases where we had reasons to suspect that our initial photometric calibration was not of high quality, we did find indeed photometric shifts as large as $\Delta r' \sim 0.5$ mag. This is why we decided to apply these corrections to our photometry, with the SDSS one taking priority over CMC.

Table 2 lists the ultimate photometric calibration data used in each field.

Armed with this refined calibration in r' , we then exported this into the g' and i' bands by constructing a $g' - r'$ vs $r' - i'$ colour-colour diagram. We then compared this to a calibrated colour-colour sequence pattern that was constructed using WFC observations of ELAIS fields. Shifts were applied to g' and i' WFC magnitudes as to match both. These shifts were propagated to all magnitudes listed in this paper.

The bottom line is that we believe our photometry to be better than 0.1 mag in the majority of our fields and certainly better than 0.2 mag for all of them. In section 5.5, where we analyze the X-ray-to-optical flux ratio, we use the quantity $\log f_{opt}$, which has a maximum error due to these calibration uncertainties well below 10%.

3.3. Astrometric calibration

Astrometric calibration of the WFC was performed using the Cambridge Astronomy Survey Unit (CASU) procedures. Typically, hundreds of matches per WFC image were obtained against the APM catalogue⁷, which was used as the astrometric reference for the optical images. Specifically, a simple 6 parameter plate solution over the whole 4-CCD image was used, but accounting for a known and previously calibrated telescope distortion cubic radial term. The residuals from the plate solution, were typically below 0.2 arcsec, which is indeed good enough for identifying candidate counterparts to the X-ray sources and for blind spectroscopic observations to identify these counterparts.

It should be noted that the astrometry of the *XMM-Newton* X-ray source position was registered against the USNO A2 (Monet et al., 1998) source catalogue (Carrera et al., 2007), and that the optical astrometry refers to a different astrometric system. In order to ensure that this does not lead to artificial mismatches, we measured the USNO-APM shifts in every *XMM-Newton* field by cross-correlating both source catalogues in the corresponding region. The shifts were significant in most cases but small, typically < 0.5 arcsec, which is less than the statistical accuracy in the X-ray source positions (0.6 arcsec averaged over the whole XMS sample). The positions of bright sources which were severely saturated in our WFC images were obtained from the USNO catalogue itself and therefore do not suffer from these small APM-USNO shifts. Given the small size of these shifts and in view of the much broader overall distribution of offsets between the position of the X-ray source and its optical counterpart (see Fig. 2) we conclude that the use of these two different astrometric reference frames does not affect in any noticeable way the results presented in this paper.

4. Identification of the XMS sources

In order to search for candidate counterparts of the X-ray sources, we normally used the r' -band WFC image. Optical source lists for these images were generated with the CASU procedures.

Counterparts for the X-ray sources were searched for in the optical image lists. Candidate counterparts had to be either within the 5 statistical errors (at 90% confidence) of the X-ray position or within 5 arcsec from the position of the X-ray source. This last criterion was used to accommodate any residual systematics in the astrometric calibration of the X-ray EPIC images.

⁷ <http://www.ast.cam.ac.uk/~mike/apmcat/>

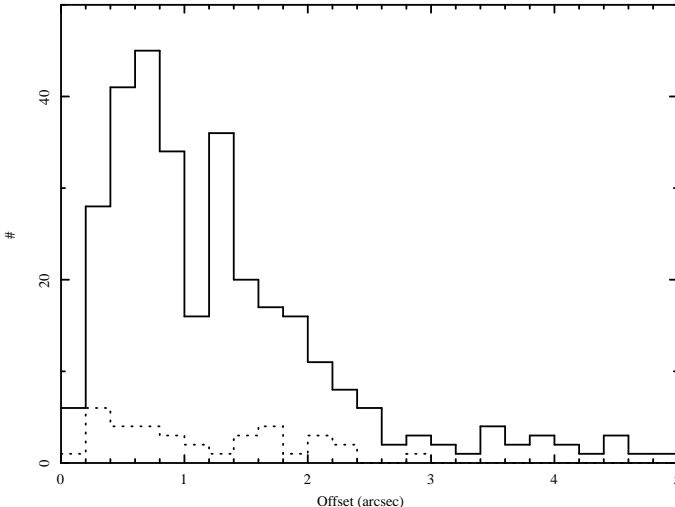


Fig. 2. Histogram of the distances from the optical source to the X-ray source centroid. The continuous line is for all sources with a counterpart and the dotted line for those with a likely counterpart without spectroscopic confirmation.

As reported in Barcons et al. (2002) this resulted in a vast majority of the XMS sources having a single candidate counterpart. There are a few exceptions to this. In a few cases (15), the position of the X-ray source happened to fall in the gaps between CCDs in the WFC images. The strategy adopted to image in all optical filters with the same aim point, which allowed us to obtain reliable optical colour information for the vast majority of the sources, also implied that for these few sources there is no optical image in any of the optical filters covering the region around these X-ray sources. In a fraction of these sources (14 out of 15), the candidate counterpart was found by considering other optical imaging data, mostly the USNO A2 catalogue, or complementary imaging data.

Also, in a modest amount of sources (78), there was more than one single candidate counterpart formally complying with our proximity criteria. But in 70 out of these 78 the optical source closest to the X-ray source position was also brightest and we adopted that as the likely counterpart. Given the brightness of the optical counterparts $r' < 22$ and the small region searched for around every X-ray source, we are confident that the number of spurious associations is insignificant in this sample.

Figure 2 shows the histogram of the X-ray to optical angular separations for the sources spectroscopically identified and for those where a unique candidate counterpart is found but without a spectroscopic identification. The distribution peaks at small separations ($\sim 2''$). Integrating this distribution outwards shows that in 68%, 90% and 95% of the cases the optical counterpart lies closer than 1.5'', 2.4'' and 3.6'' from the X-ray source respectively. Although the histogram of unidentified sources looks slightly more disperse than that of the identified ones, all candidate optical counterparts fall within 3'' from the position of the X-ray source.

There are a total of five sources that have no candidate counterpart in any of our optical images. For a further 3 sources, finding a candidate counterpart required special strategy: in one case a counterpart was only found in the K -band (XMSJ 122143.6+752238), and in a further two cases the very faint optical counterparts were only detected via imaging with the VLT (XMSJ 225227.6-180223, in the I band) and Subaru (XMSJ 021705.4-045654, with $R = 25.60$) telescopes.

4.1. Optical spectroscopy

Searches for information on the XMS candidate counterparts in existing catalogues gave useful information (i.e., nature of the source and redshift) only for a handful of objects. Identifications for a few other X-ray sources were provided to us by the Subaru/*XMM-Newton* Deep Survey project (M. Akiyama, private communication) and by the *XMM-Newton* Bright Source Survey (Della Ceca et al., 2004). That means that the vast majority of the XMS sources were previously unidentified and required optical spectroscopy.

Optical spectroscopy was conducted in a number of ground-based optical facilities, following the strategy presented in Barcons et al. (2002). The low surface density in the sky of the XMS sources ($\sim 100 \text{ deg}^{-2}$) makes the use of multi-object slit-mask spectrographs not particularly efficient. Part of the identifications were performed using a fibre spectrometer (AUTOFIB2/WYFFOS) which covers a much larger solid angle in the sky and therefore is better suited for the identification work.

The main limitation of the fibre spectrometers in obtaining the spectrum of faint sources resides in the subtraction of the sky which enters the fibres along with the light from the target objects. Wider fibres make this problem worst. This limits the ultimate sensitivity of the spectrometer, which for our exposure times and observing conditions was rarely good enough for magnitudes fainter than $r' \sim 20.5$.

Therefore, despite the larger solid angle covered by fibre spectrometers, the distribution of optical magnitudes in the XMS source candidate counterparts calls for the use of single object long-slit spectroscopy. A number of such spectrometers were used in a variety of ground-based telescopes, with apertures from 2.5m to 8.2m.

Table 4 lists the telescopes and observatories that were used, along with the specific spectrometers, with specification of the wavelength range, the slit width (or fibre width when applicable) along with the measured spectral resolution using unblended arc lines (or a sky line in the case of the fibre spectrometer). The spectral reduction process is standard and was described in Barcons et al. (2002). The final spectra will be available under <http://www.ifca.unican.es/~xray/AXIS> and in the long term in the *XMM-Newton* Science Archive⁸ under the 2XMM catalogue.

It is worth recalling that these spectra are meant only to be reliable for *identification* purposes, i.e., the spectrophotometric calibration has only been performed at best in relative terms (i.e., up to an absolute normalisation factor). Even more, in the fibre spectra and in some of the long-slit spectra which were not taken with the slit aligned to the parallactic angle, differential refraction will cause the overall large-scale shape of the spectrum to be incorrect. None of these facts hamper the identification of the spectral features that we used in this paper, which is based on broad and/or narrow emission lines and on absorption bands, but not on broad-band features like the 4000 Å break. However we want to caution against the use of these spectra to measure line fluxes or line ratios because of the above limitations.

4.2. Classification of the sources

Based on the optical spectroscopy, we classify the counterparts to the XMS X-ray sources as in Barcons et al. (2002). Extragalactic sources exhibiting broad emission lines (velocity

⁸ <http://xmm.vilspa.esa.es/xsa>

Table 4. List of spectroscopic setups relevant to this sample.

Telescope	Instrument	Spectral range (Å)	Slit width (arcsec)	Spectral resolution ^a (Å)	Comments
WHT/ORM	AUTOFIB2/WYFFOS	3900-7100	2.7 ^b	7	Fibre
WHT/ORM	AUTOFIB2/WYFFOS	3900-7100	1.6 ^b	6	Fibre
WHT/ORM	ISIS	3500-8500	1.2-2.0	3.0-3.3	Long slit
TNG/ORM	DOLORES	3500-8000	1.0-1.5	14-15	Long slit
NOT/ORM	ALFOSC	4000-9000	1.0-1.5	4	Long slit
3.5m/CAHA	MOSCA	3300-10000	1.0-1.7	24	Long slit
UT1/ESO	FORS2	4400-10000	1.0	6-12	Long slit

^a Measured from unsaturated arc lines^b Width of individual fibres

widths in excess of $\sim 1500 \text{ km s}^{-1}$) are classified as BLAGN (Broad Line Active Galactic Nuclei); those exhibiting only narrow emission lines are termed NELG (Narrow Emission Line Galaxies); those with galaxy spectra without obvious emission lines are classified in principle as Absorption Line Galaxies (ALG). Out of the latter, we distinguish two classes of exceptions: two of the sources with a galaxy spectrum without emission lines were previously catalogued as BL Lac objects and we classify them as such; if a qualitative inspection of the optical images show obvious evidence for a galaxy concentration we then classify the source as a cluster (Clus). Finally all X-ray sources with a stellar spectrum are labeled simply as "Star".

This classification is simple to perform, but it lacks in some cases a more detailed physical description of the source. This is particularly true in the case of the NELG, because no line diagnostics are performed to check whether the object hosts an AGN or not. The reason is that due to the rather wide redshift range spanned by these sources and the rather narrow wavelength coverage of the optical spectra (particularly for the fibre spectroscopy) the number of lines detected is small. Therefore it happens that typical diagnostic lines drift out of the spectrum with redshift. In addition, the quality of the spectra are in most cases not good enough to detect weak lines necessary for these diagnostics. In fact the NELG are likely to be a mixed bag of type-2 AGN and star forming galaxies. In the discussion of the various samples we use the X-ray luminosity as an indicator of the presence of an AGN in these objects.

The second limitation of this simple classification is in the case of clusters. The very small number of X-ray sources identified as clusters (2) is not a real property of the X-ray sky at these flux levels, but an artifact of the detection and classification method. The detection method for X-ray sources is designed for point sources and might be missing a number of extended X-ray sources. In addition, in several optical images, the presence of a cluster of galaxies might not be obvious and the source might have been identified as a galaxy with or without emission lines.

The third and final limitation is in the stellar content. The stars that we identify have a varied range of spectral properties, but this is not explored in the present paper.

Redshifts have been measured by matching the most prominent features in emission or absorption to sliding wavelengths of these features. Templates for QSO and galaxies with a range of spectroscopic classes were used to assist in the generation of first guesses when necessary, especially when there were no prominent features.

Table 5 displays the full list of the 318 XMS sources, along with optical magnitudes of their counterparts, and the identifications.

5. The XMS X-ray source populations

5.1. General

The breakdown of the identifications in the 4 XMS samples is shown in Table 6. The completeness of these identifications is higher for the XMS-S (95%) and XMS-X (92%) than for the XMS-H (83%) and XMS-U (86%). There are several reasons for that, the most important one being that the XMS was originally conceived around the 0.5-4.5 keV band to optimise the *XMM-Newton* EPIC sensitivity and therefore the identification strategy has been specially successful in this band.

In particular, and as we will show later, the *Hard* and *Ultra-hard* samples contain a higher fraction of sources with a higher X-ray-to-optical flux ratio and therefore more sources have optically fainter counterparts. Given the limitations of the access to 8-10m aperture class telescopes, in practice this means that the identification incompleteness is also biased. This implies that the fraction of unidentified sources is likely to be richer in potentially obscured objects than the average.

The results for the XMS-X are particularly robust and in fact their robustness can be verified by using what we might call the "Southern" subset of the XMS-X. This is due to the fact that virtually all sources in this sample which are accessible from the VLT at ESO were observed in September 2005 during the 075.A-0336 run and the vast majority of them were identified. Table 6 also displays the numbers of identified targets in fields below a declination of $+20^\circ$ in the XMS-X sample. In this sample, at the price of reducing the size from the parent sample to $\sim 60\%$, we raise the identification fraction to over 98% (only 4 sources out of 167 remain unidentified).

A first glance at the overall source population that we are sampling, can be seen in Fig. 3, where we have plotted the optical magnitude (typically r' , but R when r' is not available), as a function of 0.5-4.5 keV X-ray flux.

5.2. Stellar versus extragalactic content

Despite the high-galactic latitude selection of the *XMM-Newton* fields used in the XMS, a few of our X-ray sources have been identified as stars. A detailed study of the stellar content of the XMS is beyond the scope of this paper, but similarly to what is found in the *XMM-Newton* Galactic Plane Survey (Motch et al., in preparation) most of them will be active coronal stars.

The current landscape of X-ray surveys indicates that the stellar content at high galactic latitudes decreases at faint fluxes. Since it is unlikely that any stellar X-ray source has escaped identification in the XMS survey, we are in a position to quantify this statement as well as to compare the stellar populations when selected at different energy bands.

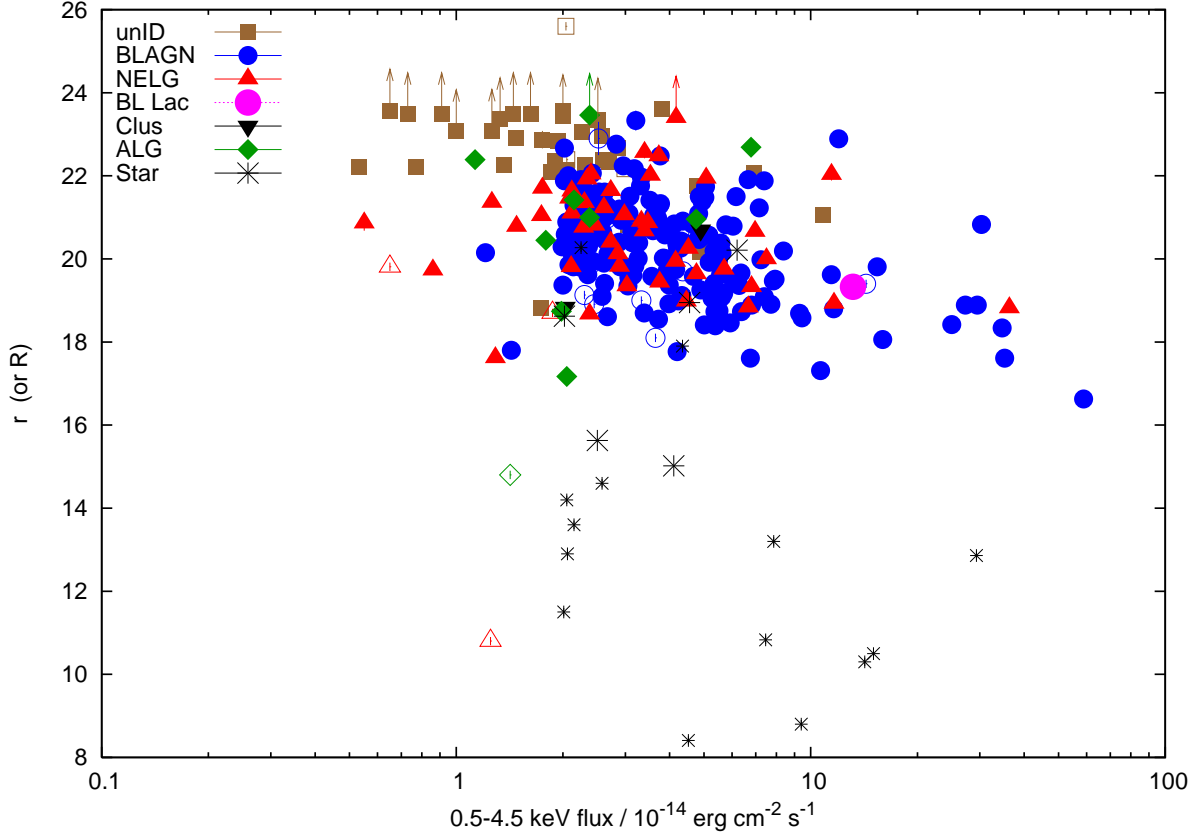


Fig. 3. Optical magnitude versus 0.5-4.5 keV flux for the XMS sources. The optical magnitude shown is r' (filled symbols) when available, and otherwise R (hollow symbols). Upward arrows denote lower limits in the magnitude derived from the lack of optical counterparts in the WFC r' band image, but note that several of these sources have counterparts in other optical bands.

Table 6. Summary of the identifications of the various XMS samples

Sample	Total	BLAGN	NELG	ALG	BL Lac	Clus	Star	Unid
XMS-S	210	150	26	6	2	1	15	10
XMS-X	284	192	38	7	2	2	20	23
XMS-X (South)	167	120	25	4	0	1	13	4
XMS-H	159	85	34	7	2	1	3	27
XMS-U	70	41	15	2	2	0	0	10

The XMS-X sample contains a total of 20 stars, which represent $7^{+3}_{-2}\%$ of the sample (henceforth errors on fractions are of 90% confidence and assuming a binomial distribution). If we split the XMS-X sample between bright (0.5-4.5 keV flux above $3.3 \times 10^{-14} \text{ erg cm}^{-2} \text{ s}^{-1}$) and faint (below the same flux) X-ray sources, the whole sample splits in two approximately equal halves (143 bright and 141 faint X-ray sources). The fraction of stars (8) in the faint sample is then $5.5^{+4.5}_{-2.5}\%$ and the fraction of stars (12) in the bright sample is $8.5^{+4.5}_{-3}\%$.

López-Santiago et al. (2007) have explored the stellar content of the BSS (Della Ceca et al., 2004), finding 58/389 ($15 \pm 3\%$) stars in the 0.5-4.5 keV sample. Combined with our own measurements on the XMS-X, this shows that there is a decrease in the stellar content when going to fainter X-ray fluxes.

It is also interesting to compare the fraction of stars in the various XMS samples. The soft XMS-S sample contains 15 stars, which represent $7^{+4}_{-2}\%$ of the sample, similar to the XMS-X. The stellar content in the XMS-X and XMS-S samples is very similar.

Stars are much rarer in the XMS-H and XMS-U samples: the XMS-H contains only 3 stars ($2^{+2.5}_{-1}\%$) and the XMS-U contains no stars whatsoever (< 4% at 90% confidence). In this case we are totally confident that we are not missing any stars, as all unidentified sources in the XMS-H and XMS-U samples are optically extended. The small stellar content in these samples is not a surprise, as most of our stars are seen in X-rays because of their active coronae, which have X-ray spectra that are dominated by soft X-ray line emission and peak around 1 keV.

5.3. Luminosity and Redshift distributions

The vast majority of XMS sources are extragalactic. We have computed the X-ray luminosities of the extragalactic sources (not corrected for absorption) and these are represented in Fig. 4 as a function of redshift for each of the XMS samples.

A visual inspection of these $L - z$ relations reveals that all but a few sources optically classified as NELGs have X-ray luminosities in the corresponding band in excess of $10^{42} \text{ erg s}^{-1}$, and are therefore most likely to host a hidden AGN. With very

few exceptions, NELGs in our survey are therefore type 2 AGN. In fact, the 2-10 keV luminosity of 6 such objects exceeds 10^{44} erg s $^{-1}$ and therefore qualify as type 2 QSOs in standard X-ray astronomy parlance.

The X-ray luminosity of a fraction of sources that we classified as ALG, also exceeds 10^{42} erg s $^{-1}$. Specifically the number of ALG that exceed this luminosity threshold are 4 out of 7 in the most numerous and complete XMS-X. Such sources are often referred to as X-ray Bright Optically Normal Galaxies (XBONGS) and when studied in detail are invariably seen to host an AGN, which is either heavily obscured, or of low luminosity and in any case outshone by the host galaxy, as shown by Severgnini et al. (2003), Rigby et al. (2006) and Caccianiga et al. (2007).

We also find a couple of X-ray sources classified as ALG with low X-ray luminosities ($\sim 10^{40}$ erg s $^{-1}$). In at least one case (XMSJ 084221.6+705758) the position of the X-ray source falls in the outskirts of the galaxy, and therefore is likely to be a candidate for an Ultra-luminous X-ray source. Watson et al. (2005) have discussed some of these sources in the context of the Subaru/*XMM-Newton* Deep Survey.

The overall luminosity distribution in all four samples is centered around 10^{44} erg s $^{-1}$, which means that the sample contains both Seyfert-like AGN and QSOs. This value is also where the AGN X-ray luminosity function exhibits a knee and therefore where most of the X-ray volume emissivity comes from.

The redshift distribution is displayed in Fig. 5 for the four samples. The peak of the BLAGN population in the XMS-S and XMS-X samples is around $z \sim 1.5$ which is not far from the one found in deeper surveys. However, the redshift cutoff at around $z \sim 3$ is due to the limited depth of the XMS that fails to find the higher redshift AGN revealed by deeper surveys.

The contribution from NELG and ALG, most of which are obscured AGN, peaks at low redshift, typically $z < 0.5$. This is lower than the peak revealed by deep surveys, due to the modest depth of the survey. What is worth noting, however, is the comparison between the various XMS samples. Comparing the redshift distribution for the softer XMS-S sample to the hard XMS-H sample (which are drawn from a different parent population according to the Kolmogorov-Smirnov test which gives a probability of 10^{-13} for the null hypothesis) shows that with a similar sky density the hard sample misses an important fraction of unobscured AGN (BLAGN) at high redshift but includes virtually all the obscured objects. The redshift distribution is consequently shifted to lower values. We next discuss in more detail the relative fraction of obscured AGN.

5.4. Obscured versus unobscured AGN

The fraction of obscured AGN is known to have a strong dependence on the X-ray selection band and also on the depth of the survey. Typically soft X-ray selection misses a large fraction of obscured (and therefore likely absorbed in the X-ray band) AGN. Deeper X-ray surveys, even with soft X-ray sensitivity only, have also produced increasingly large fractions of obscured AGN.

The broad bandpass of *XMM-Newton* allows us to study the fraction of obscured AGN as a function of selection band and depth, at the intermediate fluxes sampled by the XMS. A detailed multi-wavelength study of the XMS survey, combining X-ray spectral information, optical colours and data at infrared and radio wavelengths is in preparation (Bussons-Gordo, in preparation).

For the purposes of the current discussion, we now classify as an AGN any extragalactic X-ray source whose 2-10 keV X-ray luminosity exceeds 10^{42} erg s $^{-1}$ and is not obviously associ-

ated with a cluster of galaxies. This stems from the observational fact that in the local Universe all sources more luminous than this are at the very least suspected to harbour an AGN. A potential limitation of our classification, and therefore of our estimates of the fraction of optically obscured sources among AGN, comes from the limited quality of the optical spectra, in particular if weak broad emission lines are present. This is illustrated in the BSS (Caccianiga et al 2007,Della Ceca et al, in preparation) where some of the sources originally classified as ALG or NELG turned out to have "elusive" broad emission lines. For the purposes of this paper, an AGN which does not display an obvious dominant broad emission line, is considered as an obscured AGN.

The sources that we have classified as BLAGN are unobscured AGN. In fact, a fraction of these (around 10 per cent) display X-ray photoelectric absorption (Mateos et al., 2005a,b), but whatever the nature of these absorbers, they do not contain enough dust to obscure the broad line regions of these AGN, and in this context we will not consider these to be obscured AGN.

Among the sources classified optically as NELG or ALG, an important fraction of them are AGN according to the above scheme, and we term these as obscured AGN, since their Broad Line Region is not seen. It must be stressed anyhow that obscured AGN are expected to follow the AGN unified model predictions in the sense that they host the same central engine as an unobscured AGN, but that due to the presence of dust the Broad Line Region is heavily reddened and therefore not seen. Photoelectric absorption is expected in their X-ray spectrum (and certainly seen in most cases), but in about half of AGN without broad emission lines X-ray absorption is undetected (Mateos et al., 2005a). There are a number of hypotheses that can explain this mismatch, some of them dealing with the structure of the AGN itself, and not with real obscuration of a standard AGN (Mateos et al., 2005b). However, this discussion is beyond the scope of this paper, and we stick to the standard interpretation that the lack of broad emission lines is equivalent to obscuration.

A potential problem in the study of the fraction of the obscured objects among the AGN population arises because the fraction of unidentified X-ray sources is higher for optically fainter sources and these are more likely to be obscured. There is an indication of this being true, as most of their optical counterparts appear extended and therefore dominated by host galaxy light rather than by the nucleus.

For the XMS-X, we find 42 optically obscured AGN out of a total sample of 236 identified AGN, which represent $18^{+4}_{-4}\%$. This fraction is rather robust as it remains virtually unchanged if we restrict its estimate to the "South" XMS-X sample complete sample ($20^{+5}_{-5}\%$).

The fact that this fraction is indeed much smaller than what is expected from local Universe studies, where obscured AGN outnumber unobscured ones by a factor of 3, is indeed due to the fact that obscuration comes along with photoelectric X-ray absorption which suppresses X-rays, particularly in the soft band. This implies that at harder X-ray energies there should be a higher fraction of obscured AGN. Although this is what qualitatively emerges from existing X-ray surveys, the size and combination of various selection bands on the XMS can provide a quantitative measurement of these effects. There is also some qualitative perception that the fraction of obscured AGN increases substantially when going deeper in a given X-ray energy band. In what follows we attempt to test these statements.

If we divide again the XMS-X sample in two approximately equal halves of faint and bright X-ray sources (0.5-4.5 keV

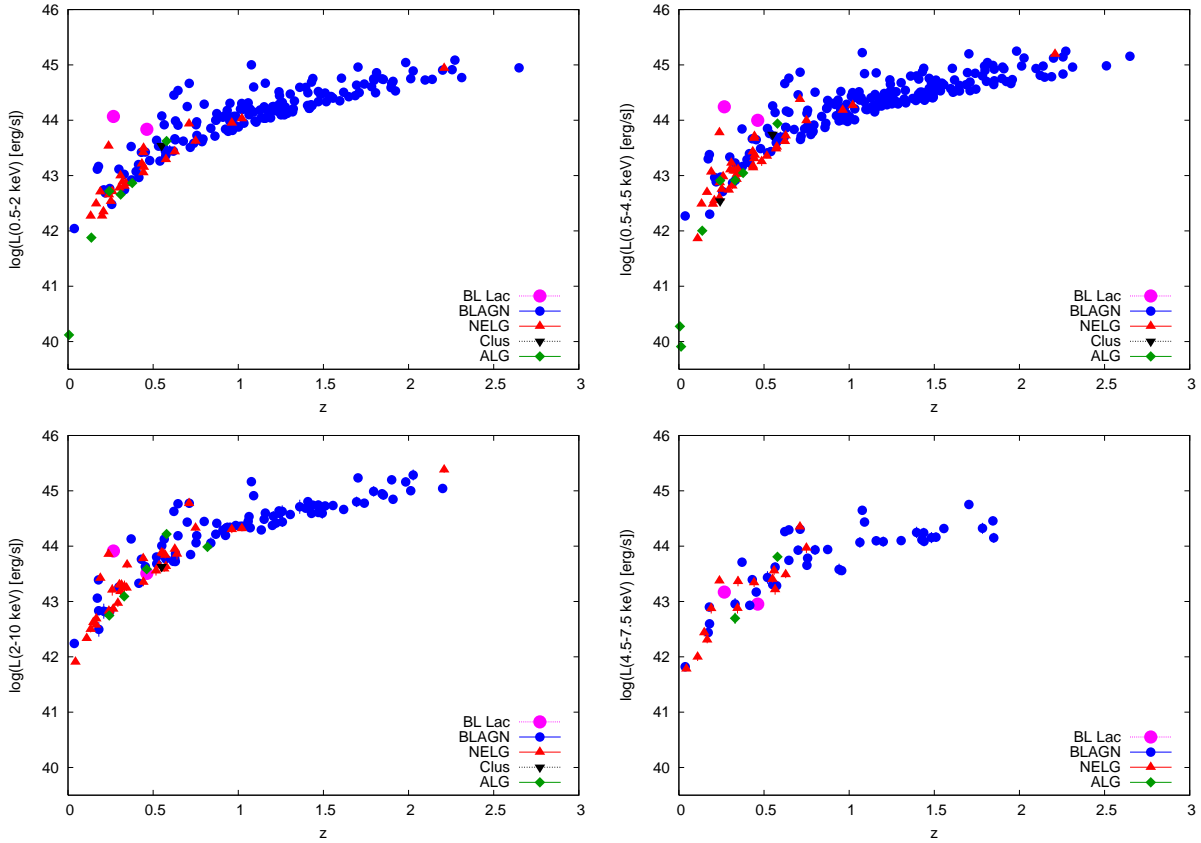


Fig. 4. X-ray luminosity in the selection band versus redshift for extragalactic sources in each one of the XMS samples. Top left is for the XMS-S, top right for the XMS-X, bottom left for the XMS-H and bottom right for the XMS-U.

fluxes below and above $3.3 \times 10^{-14} \text{ erg cm}^{-2} \text{ s}^{-1}$), among the identified sources obscured AGN represent $17_{-5}^{+6}\%$ of the faint AGN and $19_{-5}^{+6}\%$ of the bright AGN. This lack of flux dependence, is confirmed when we restrict it to the "South" XMS-X complete sample ($20_{-6}^{+9}\%$ and $19_{-6}^{+9}\%$ of obscured AGN for faint and bright sources respectively). This is within errors of what comes out if we assume that *all* unidentified sources in the XMS-X sample are obscured AGN, in which case the fraction of obscured AGN would be slightly higher ($25_{-4}^{+5}\%$) and independent of flux. Incidentally, comparison of this fraction to the $\sim 20\%$ of obscured AGN in the South XMS-X sources, shows that despite being an important obscured AGN component among the unidentified XMS-X sources, there might be some type 1 AGN among them. We will return to this point later when discussing X-ray-to-optical flux ratios.

In the XMS-S the fraction of obscured AGN is $17_{-4}^{+5}\%$, which is very marginally smaller than in the XMS-X sample. This fraction remains unchanged when we split the XMS-S in faint and bright sources.

Things change significantly when we deal with hard X-ray selected sources. The identified sources in the XMS-H sample contain $35 \pm 7\%$ obscured AGN which could be as high as $45 \pm 7\%$ if all unidentified sources are obscured AGN. None of these figures change between XMS-H bright and faint X-ray sources.

There are no dramatic changes when we use the XMS-U sample with respect to the XMS-H sample: obscured AGN represent $31_{-6}^{+7}\%$ of the AGN population which might be slightly higher if all unidentified sources are obscured AGN ($43_{-6}^{+7}\%$).

In summary, in soft X-ray selected samples at intermediate fluxes, about $\sim 20 - 25\%$ of the AGN are obscured, and

this applies to both 0.5-2 keV and 0.5-4.5 keV selection. The *XMM-Newton* BSS (Della Ceca et al., 2004), which is also selected in the 0.5-4.5 keV band but at brighter fluxes, finds a slightly smaller fraction of obscured AGN, in the range of 6 to 14%. In the opposite flux direction, the *ROSAT* ultra-deep survey (Lehmann et al., 2001), which contains 94 X-ray sources with a 0.5-2 keV flux down to $1.2 \times 10^{-15} \text{ erg cm}^{-2} \text{ s}^{-1}$ and identified to 90% completeness, also found $\sim 20\%$ of obscured objects among the AGN population (13 out of 70).

The fraction of obscured AGN goes up to $\sim 35 - 45\%$ for hard X-ray selected samples at intermediate fluxes in the XMS. This applies equally to 2-10 keV selection and to 4.5-7.5 keV selection. This means that above 4.5 keV the sensitivity of *XMM-Newton* is not high enough, and our exposure times are not deep enough, to raise new heavily obscured X-ray sources that are not selected in the 2-10 keV band. These fractions do not appear to change with X-ray flux of the sources within the flux ranges sampled by our survey. In this case, comparison with the Hard Bright Source Survey (Caccianiga et al., 2004, Caccianiga et al., 2007, Della Ceca et al., in preparation), selected in the 4.5-7.5 keV band shows no change in the fraction of obscured AGN, which these authors quantify as 31 – 33%. The *Chandra* Multi-wavelength Survey (Silverman et al., 2005) (which goes down to 2-10 keV fluxes between 10^{-15} and $10^{-14} \text{ erg cm}^{-2} \text{ s}^{-1}$), when restricted to optically bright sources, reports that 28% of the total source sample is obscured, but its identified fraction in only 77% and therefore this fraction is most likely a lower limit.

A final point to address is the dependence of the fraction of optically obscured AGN as a function of X-ray luminosity. This fraction is reported by Barger et al. (2005) and

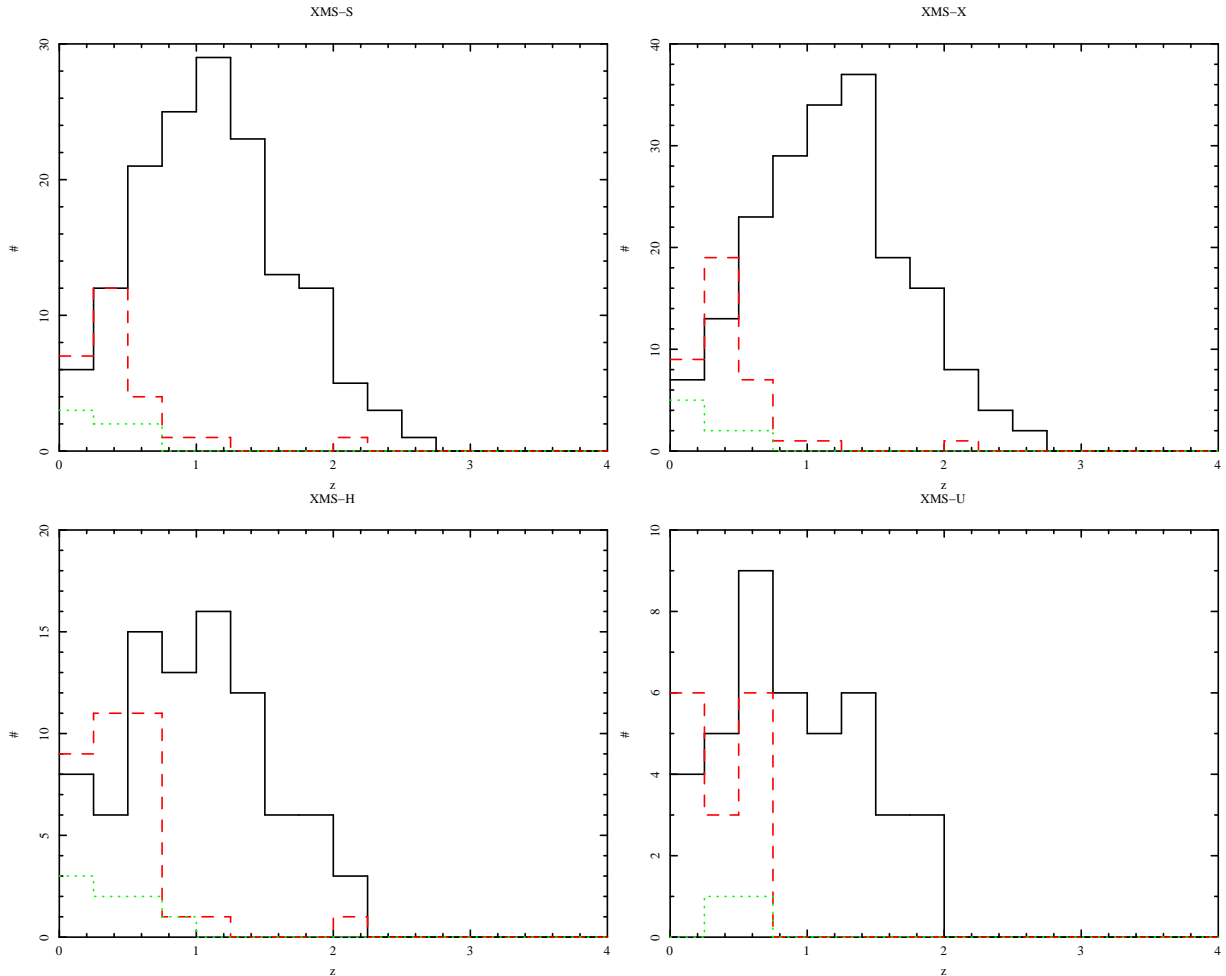


Fig. 5. Redshift histograms in each one of the XMS samples. Solid line is for BLAGN, dashed line for NELG and dotted line for ALG. Top left is for the XMS-S, top right for the XMS-X, bottom left for the XMS-H and bottom right for the XMS-U.

Gilli, Comsatri & Hasinger (2007) among others, to decrease towards high luminosities. From Fig. 4 we can see this effect clearly happening in the XMS. For the XMS-H the fraction of optically obscured extragalactic objects with 2–10 keV luminosity between 10^{42} and 10^{44} erg s $^{-1}$ is 62% (34 out of 55 objects) and above 10^{44} erg s $^{-1}$ is only 9% (6 out of 70 objects). These numbers are consistent, within errors, with those quoted by Barger et al. (2005) and Gilli, Comsatri & Hasinger (2007). However, Fig. 4 itself shows the very restricted coverage of the luminosity-redshift plane of a single flux-limited survey. We believe that addressing this issue needs the combination of multiple surveys covering different depths and solid angles in a way that samples evenly the luminosity-redshift plane.

5.5. X-ray to optical flux ratio

The X-ray to optical flux ratio has been used in various surveys as a proxy for obscuration. Similarly to other papers (Krumpe et al., 2007; Cocchia et al., 2007), we use as a proxy for optical flux that in the r' band and therefore compute $\log f_{opt} = -0.4r' + \log(f_{r'0}\delta\lambda)$, where $f_{r'0} = 2.40 \times 10^{-9}$ erg cm $^{-2}$ s $^{-1}$ Å $^{-1}$ is the zero-point for r' and $\delta\lambda = 1358$ Å is the FWHM of the r' filter. Note that this yields $X/O = \log(f_X/f_{opt}) = \log(f_X) + 0.4r' + 5.49$, where f_X is the 2–10 keV flux in erg cm $^{-2}$ s $^{-1}$, not corrected for Galactic absorption (the correction is insignificant at the XMS Galactic latitudes).

Typically, unobscured type 1 AGN have $-1 < X/O < 1$, and therefore sources with X-ray to optical flux ratio in excess of 10 have been considered as likely obscured AGN.

We have excluded from this analysis those sources for which we have no reliable r' magnitudes, to avoid uncertainties. We attempted to calibrate the R versus r' relation, where the R magnitudes are mostly extracted from the literature and the USNO A2 catalogue. Specifically, Table 5 contains 105 BLAGN and 30 NELG for which we have both R and r' . Formally, $\log f_R$ versus $\log f_{r'}$ yields an offset of -0.30 for BLAGN and -0.49 for NELG, but in both cases the scatter is very large (0.25 dex). Therefore, by adding into this analysis those sources for which only R is available, we would be expanding considerably their uncertainties and therefore we decided to ignore these sources.

We have studied the fraction of obscured AGN in the various XMS samples. This is best seen in Fig. 6, where we find the vast majority of our objects to lie in the “normal” type 1 AGN domain $-1 < X/O < 1$. However, we also note that a fraction of XMS sources have extreme values of X/O . Values below -1 are usually dominated by stars.

Far more important is the other extreme $X/O > 1$ where obscured AGN are expected. Table 7 shows the numbers and fractions of obscured AGN in the various XMS samples and in 3 ranges of X/O . A difficulty is how we deal with lower limits to optical fluxes of various sources, where there is no detection in the WFC image, but only an upper limit in their magnitude from

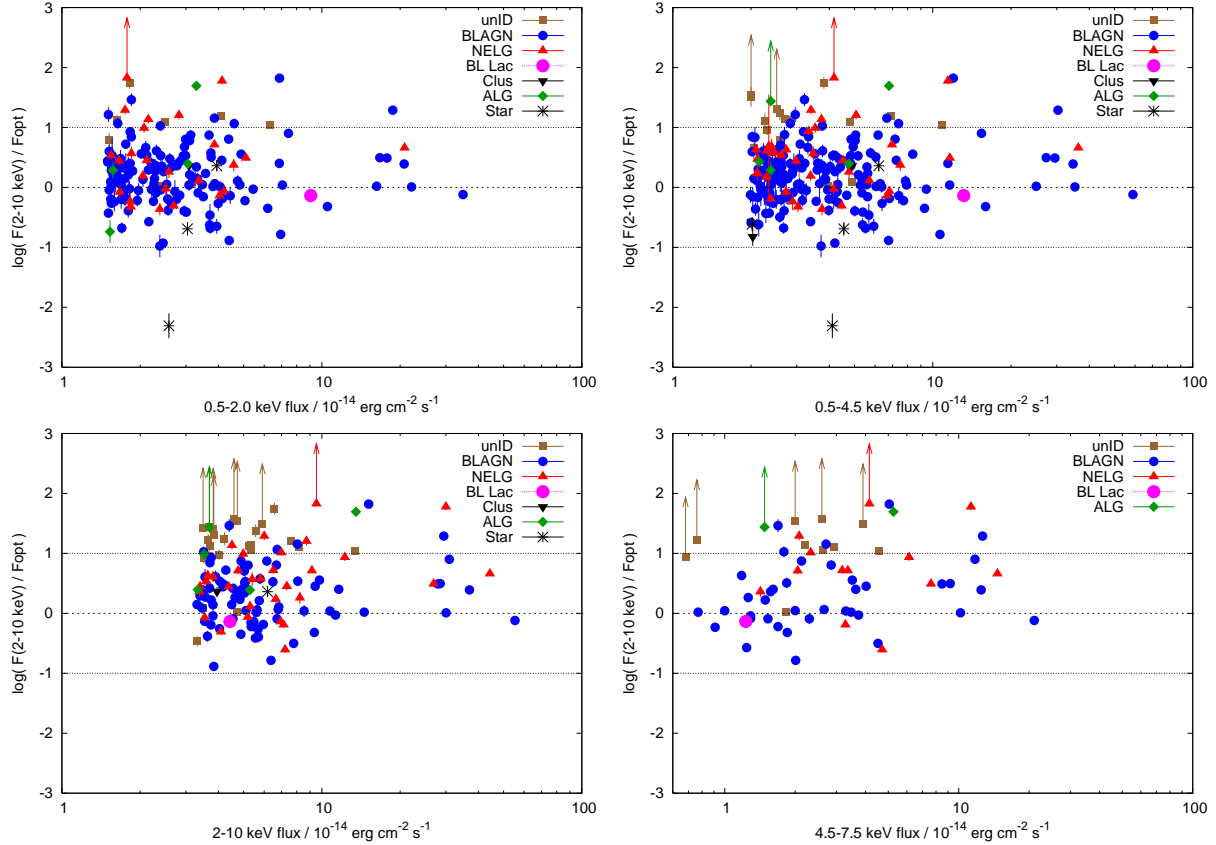


Fig. 6. X-ray to optical flux ratio as a function of X-ray flux in the corresponding X-ray band for all 4 XMS samples. Only those sources with known counterpart, which has a measured value (or a lower limit) of r' from our WFC imaging is included. In this way we miss a number of sources in each sample, but we avoid uncertain conversion factors between different bands. Top left is for the XMS-S, top right for the XMS-X, bottom left for the XMS-H and bottom right for the XMS-U. Symbols are as in Fig. 3

the sensitivity of the corresponding image. There are a number of uncertainties on this, including the likely possibility that the undetected counterpart is optically extended and therefore might be actually brighter (in integrated magnitude) than the quoted lower limit. For these sources (which are actually very few) we have used the lower limit in X/O as if it were a real detection.

The first result that becomes evident from Table 7 is the fact that the fraction of sources with $X/O > 1$, and therefore potentially obscured, varies substantially between samples. For the XMS-S, we find only 5 sources with $X/O > 1$ among a sample of 180 with measured X/O which represent only $3 \pm 2\%$. This percentage grows to $7^{+4\%}_{-2\%}$ (17/245) for XID-X and grows even further for the XMS-H to $17^{+7\%}_{-5\%}$ (23/138) (for the XMS-U the numbers are too small to reach any conclusion). It is therefore clear that the fraction of sources with large X/O goes up from a small few per cent in the 0.5-2 keV selected XMS-S sample to 20% in the 2-10 keV selected XMS-H sample, with XMS-X in between. Note that these percentages have to be revised slightly downwards, as we are missing r' magnitudes of most of the stars (more abundant in the softer samples) which are totally saturated in our WFC images.

We see from Table 7 that the fraction of obscured AGN among the $X/O > 1$ sources is higher than in the whole sample, and this holds for all XMS samples. The second fact that can be seen by inspecting Table 7 is that in the XMS-H the fraction of obscured AGN amongst the $X/O > 1$ sources could be as high as 90% if all unidentified sources are obscured AGN, but this percentage is lower for the XMS-S and XMS-X.

Table 7. Fraction of obscured AGN in the various XMS samples. (f_{obsc}) is the fraction actually measured and (f_{obsc}^*) the fraction that would result under the assumption that all unidentified sources are obscured AGN.

$\log(F(2-10\text{keV})/F_{r'})$	f_{obsc}	f_{obsc}^*
XMS-S		
-1.0 : 0.0	$17^{+8\%}_{-8\%}$ (14/84)	$18^{+8\%}_{-8\%}$ (15/85)
0.0 : +1.0	$17^{+8\%}_{-8\%}$ (14/81)	$25^{+8\%}_{-7\%}$ (22/89)
> +1.0	$25^{+49\%}_{-15\%}$ (1/4)	$40^{+41\%}_{-21\%}$ (2/5)
XMS-X		
-1.0 : 0.0	$12^{+9\%}_{-5\%}$ (8/65)	$14^{+8\%}_{-6\%}$ (9/66)
0.0 : +1.0	$20^{+6\%}_{-6\%}$ (29/146)	$25^{+6\%}_{-5\%}$ (39/156)
> +1.0	$36^{+29\%}_{-17\%}$ (4/11)	$59^{+19\%}_{-17\%}$ (10/17)
XMS-H		
-1.0 : 0.0	$21^{+16\%}_{-9\%}$ (6/28)	$24^{+16\%}_{-10\%}$ (7/29)
0.0 : +1.0	$28^{+9\%}_{-7\%}$ (22/78)	$34^{+9\%}_{-8\%}$ (29/85)
> +1.0	$50^{+25\%}_{-18\%}$ (6/12)	$74^{+14\%}_{-14\%}$ (17/23)
XMS-U		
-1.0 : 0.0	$14^{+15\%}_{-7\%}$ (4/29)	$17^{+17\%}_{-8\%}$ (5/30)
0.0 : +1.0	$39^{+22\%}_{-15\%}$ (7/18)	$50^{+19\%}_{-14\%}$ (11/22)
> +1.0	$50^{+40\%}_{-25\%}$ (2/4)	$50^{+40\%}_{-25\%}$ (2/4)

But we can also look at this fact from a different point of view, which is that there are unobscured AGN with $X/O > 1$. There are at least 3/5, 7/17, 6/23 and 2/4 unobscured AGN with $X/O > 1$ in the XMS-S, XMS-X, XMS-H and XMS-U samples respectively, which represent somewhere between one fifth

and one half of the corresponding sample with a selection cut at $X/O > 1$. The nature of these BLAGN with $X/O > 1$ will be investigated in future papers.

6. Conclusions

In this paper we have presented the *XMM-Newton* Medium sensitivity Survey XMS, and extracted a number of robust quantitative conclusions about the population of high Galactic latitude X-ray sources at intermediate flux levels. We have argued that given the completeness of our identifications and the relatively large size of the XMS samples, these conclusions can be safely exported to a much larger X-ray source catalogue like 2XMM.

Our conclusions can be summarized as follows:

1. The high galactic latitude X-ray sky at intermediate flux levels is dominated by AGN, which includes type-1 and type-2 AGN as well as the so-called XBONG which are likely to host a low luminosity or obscured nucleus (or both). The stellar content is less than 10% in soft X-ray selected samples, and drops to below 5% at around soft X-ray fluxes $\sim 10^{-14}$ erg cm s $^{-1}$. The stellar content in hard X-ray selected samples does not exceed a few per cent at most. Selection in 0.5-4.5 keV produces intermediate results.
 2. Given the limited sensitivity of *XMM-Newton* above a few keV -which is due to the roll over of effective area-current surveys conducted in the so-called ultra-hard band (4.5-7.5 keV) do not bring any new source population or any significant difference with respect to 2-10 keV selected surveys. Much longer exposure times would be needed to unveil any new heavily obscured population with *XMM-Newton*.
 3. Obscured AGN represent $\sim 20\%$ of the soft X-ray selected population of AGN, all the way from $\sim 10^{-13}$ erg cm $^{-2}$ s $^{-1}$ down to $\sim 10^{-15}$ erg cm $^{-2}$ s $^{-1}$, with no compelling evidence for an increase of this fraction towards fainter fluxes within this range.
 4. Likewise, obscured AGN represent $\sim 35\%$ (45% if all unidentified sources are obscured AGN) of the hard X-ray selected population of AGN, with no hint of an increase down to a hard X-ray flux $\sim 10^{-14}$ erg cm $^{-2}$ s $^{-1}$.
 5. The fraction of X-ray sources with X-ray to optical flux ratio > 10 (or $X/O > 1$ using the notation of this paper) is a mere 3% in soft X-ray selected samples, but grows to 20% in hard X-ray selected samples.
 6. Those sources with $X/O > 1$ are mostly obscured AGN, but a fraction of around 20% of them in the hard band are unobscured type-1 AGN. This means that $X/O > 1$ alone cannot be used as a proxy for obscured X-ray sources.
- Barcons, X., Carrera, F.J., Watson, M.G. et al. 2002, A&A, 282, 522
 Barger, A.J., Cowie, L.L., Muchotzky, R.F., Yang, Y., Wang, W.-H., Steffen, A.T., Capak, P., 2005, ApJ, 129, 578
 Brandt, W.N. & Hasinger, G., ARA&A, 43, 827
 Brusa, M., Zamorani, G., Comastri, A. et al., 2007, ApJ, in the press (astro-ph/0612358)
 Baldi, A., Molendi, S., Comastri, A. et al. 2002, ApJ, 564, 190
 Caccianiga, A., Severgnini, P., Braito, V., et al. 2004, A&A, 416, 201
 Caccianiga, A., Severgnini, P., Della Ceca, R. et al. 2007, A&A, submitted
 Carrera, F.J., Ebrero, J., Mateos, S., et al. 2007, A&A, in the press (astro-ph/0703451)
 Cocchia, F., Fiore, F., Vignali, C., et al., 2007, A&A, submitted (astro-ph/0612023)
 Della Ceca, R., Maccacaro, T., Caccianiga, A. et al. 2004, A&A, 428, 383
 Fabian, A.C. and Iwasawa, K., 1999, MNRAS, 303, L34
 Fiore, F., Brusa, M., Cocchia, F., et al., 2003, A&A, 409, 79
 Georgantopoulos, I., Stewart, G.C., Shanks, T., Boyle, B.J., Griffiths, R.E., 1996, MNRAS, 280, 276
 Gilli, R., Comastri, A., Hasinger, G., 2007, A&A, 463, 79
 Gioia, I. M., Maccacaro, T., Schild, R. E., Wolter, A., Stocke, J. T., Morris, S. L., & Henry, J. P. 1990, ApJS, 72, 567
 Green, P.J., et al., 2004, ApJ, 150, 43
 Hasinger, G., Burg, R., Giacconi, R., et al., 1998, A&A, 329, 482
 Hasinger, G., Altieri, B., Arnaud, M., et al. 2001 A&A, 365, L45
 Hasinger, G., Cappelluti, N., Brunner, H., et al., ApJ, in the press (astro-ph/0612311)
 Kim, D.-W., et al., 2004a, ApJS, 150, 19
 Kim, D.-W., et al., 2004b, ApJS, 600, 59
 Krumpe, M., Lamer, G., Schwone, A.D., et al., 2007, A&A, in the press (astro-ph/0612343)
 Lehmann, I., Hasinger, G., Schmidt, M., et al., 2001, A&A, 371, 833
 López-Santiago, J., Micela, G., Sciortino, S., Favata, F., Caccianiga, A., Della Ceca, R., Severgnini, P., & Braito, V. 2007, A&A, 463, 165
 Jansen, F.A., Lumb, D., Altieri, B., et al. 2001 A&A, 365, L1
 Maccacaro, T., et al. 1982, ApJ, 253, 504
 Mainieri, V., Hasinger, G., Cappelluti, N., et al., 2007, ApJ, in the press (astro-ph/0612361)
 Marconi, A., Risaliti, G., Gilli, R., et al., 2004, MNRAS, 351, 169
 Mason, K.O., Carrera, F.J., Hasinger, G., et al. 2000 MNRAS, 311, 456
 Mateos, S., Barcons, X., Carrera, F.J. et al., 2005, A&A, 433, 855
 Mateos, S., Barcons, X., Carrera, F.J. et al., 2005, A&A, 444, 79
 McHardy, I.M., Jones, L.R., Merrifield, M.R. et al., 1998, MNRAS, 295, 641
 Merritt, D. & Ferrarese, L., 2001, MNRAS, 320, L30
 Monet, D., Canzian, B., Dahn, C. et al. 1998 A Catalog of Astrometric Standards, U.S. Naval Observatory Flagstaff Station (USNOFFS) and Universities Space Research Association (USRA) stationed at USNOFFS.
 Rigby, J. R., Rieke, G. H., Donley, J. L., Alonso-Herrero, A., & Pérez-González, P. G. 2006, ApJ, 645, 115
 Schwone, A.D., Hasinger, G., Lehmann, I. et al., 2000, Astron. Nachr., 321, 1
 Severgnini, P., Caccianiga, A., Braito, V., et al., 2003, A&A, 406, 483
 Silverman, J.D., Green, P.J., Barkhouse, W.A., et al. 2005, ApJ, 618, 123
 Stocke, J. T., Morris, S. L., Gioia, I. M., Maccacaro, T., Schild, R., Wolter, A., Fleming, T. A., & Henry, J. P. 1991, ApJS, 76, 813
 Streiblyanska, A., Hasinger, G., Finoguenov, A., et al., 2005, A&A, 432, 395
 Strüder, L., Briel, U., Dennerl, R., et al. 2001 A&A, 365, L18
 Tozzi, P., Gilli, R., Mainieri, V., et al. 2006, A&A, 451, 457
 Tremaine, S., Gebhardt, K., Bender, R. et al., 2002, ApJ, 574, 740
 Turner, M.J.L., Abbey, A., Arnaud, M., et al. 2001 A&A, 365, L27
 Ueda, Y., Akiyama, M., Ohta, K., Miyaji, T., 2003, ApJ, 598, 886
 Watson, M.G., Roberts, T.P., Akiyama, M., Ueda, Y. 2005, A&A, 437, 899

Table 2. continued.

Source Name	RA (J2000)	DEC (J2000)	r_{90}^a	Sample	$S(0.5 - 2)^b$	$S(2 - 10)^b$	$S(0.5 - 4.5)^b$	$S(4.5 - 7.5)^b$	HR_2^c
XMSJ 233158.7+194440	23 : 31 : 58.7	+19 : 44 : 40.9	1.3	S X	1.51 ± 0.27	6.75 ± 1.80	2.96 ± 0.47	1.79 ± 0.66	-0.30 ± 0.12
XMSJ 233201.5+200406	23 : 32 : 01.5	+20 : 04 : 06.6	0.8	S X	1.70 ± 0.24	2.92 ± 0.74	2.95 ± 0.39	0.68 ± 0.35	-0.48 ± 0.12
XMSJ 233203.2+200626	23 : 32 : 03.2	+20 : 06 : 26.8	0.9	SHX	2.12 ± 0.31	8.08 ± 1.48	4.19 ± 0.52	2.88 ± 1.12	-0.30 ± 0.12
XMSJ 233207.3+200529	23 : 32 : 07.3	+20 : 05 : 29.6	0.6	S X	1.80 ± 0.28	1.19 ± 0.84	2.62 ± 0.39	0.28 ± 0.35	-0.75 ± 0.08
XMSJ 233209.8+194517	23 : 32 : 09.8	+19 : 45 : 17.2	0.8	SHX	3.08 ± 0.38	8.54 ± 1.96	5.27 ± 0.61	3.36 ± 0.77	-0.53 ± 0.11
XMSJ 233212.2+200557	23 : 32 : 12.2	+20 : 05 : 57.9	0.2	S X	2.96 ± 0.40	4.33 ± 1.14	4.94 ± 0.60	1.19 ± 0.77	-0.54 ± 0.10
XMSJ 233226.5+195736	23 : 32 : 26.5	+19 : 57 : 36.5	0.8	HX	1.32 ± 0.24	5.03 ± 0.92	2.60 ± 0.39	1.47 ± 0.42	-0.29 ± 0.13
XMSJ 233228.2+195809	23 : 32 : 28.2	+19 : 58 : 09.9	1.4	S	1.53 ± 0.26	1.90 ± 0.83	1.98 ± 0.37	-	-0.95 ± 0.08
XMSJ 233232.0+195116	23 : 32 : 32.0	+19 : 51 : 16.9	0.8	X	1.42 ± 0.27	1.98 ± 0.91	2.25 ± 0.41	0.97 ± 0.44	-0.63 ± 0.10
XMSJ 233232.6+195809	23 : 32 : 32.6	+19 : 58 : 09.1	0.4	SHX	3.99 ± 0.42	5.68 ± 1.66	6.38 ± 0.62	-	-0.61 ± 0.08

^a Statistical error radius at 90% confidence in the position of the X-ray source in arcsec.

^b All fluxes are quoted in units of 10^{-14} erg cm $^{-2}$ s $^{-1}$ in the corresponding band

^c Hardness Ratio defined as $HR_2 = (H - S)/(H + S)$, where S and H are exposure-time corrected count rates in the 0.5-2 keV and 2-4.5 keV bands respectively.

X. Barcons et al.: The *XMM-Newton* Medium sensitivity Survey

Table 5. continued.

X-ray source	RA_o (J2000)	DEC_o (J2000)	g'	r'	i'	R	Id ^a	Type	z
XMSJ 233158.7+194440	23 : 31 : 58.8	+19 : 44 : 39.2	23.47	22.24	21.21		Y	BLAGN	1.418
XMSJ 233201.5+200406	23 : 32 : 01.5	+20 : 04 : 06.4					Y	BLAGN	1.517
XMSJ 233203.2+200626	23 : 32 : 03.2	+20 : 06 : 27.7	21.07	20.36	20.12	19.30	Y	BLAGN	1.901
XMSJ 233207.3+200529	23 : 32 : 07.4	+20 : 05 : 29.1	22.26	21.61	21.48		Y	BLAGN	1.897
XMSJ 233209.8+194517	23 : 32 : 09.8	+19 : 45 : 17.4	20.26	19.05	18.37	19.30	Y	BLAGN	2.027
XMSJ 233212.2+200557	23 : 32 : 12.2	+20 : 05 : 58.7		21.38	20.55		Y	BLAGN	0.870
XMSJ 233226.5+195736	23 : 32 : 26.5	+19 : 57 : 40.7	23.20	21.29	20.67		Y	BLAGN	0.521
XMSJ 233228.2+195809	23 : 32 : 28.2	+19 : 58 : 08.5	20.67	18.74	18.08	17.40	Y	ALG	0.309
XMSJ 233232.0+195116	23 : 32 : 31.9	+19 : 51 : 18.9	21.12	20.30	20.11	19.90	Y	BLAGN	1.473
XMSJ 233232.6+195809	23 : 32 : 32.6	+19 : 58 : 09.2	19.65	18.73	18.82	18.70	Y	BLAGN	1.361

^a This flag means: Y if the source has been positively identified via optical spectroscopy; C if there is a single clear optical candidate counterpart from in optical images; E if there is no candidate counterpart down to our imaging sensitivity.

List of Objects

- ‘G 133-69 pos 1’ on page 3
- ‘PB 5062’ on page 3
- ‘UZ Lib’ on page 3
- ‘B2 1128+31’ on page 3
- ‘Cl 0016+1609’ on page 4
- ‘G 133-69’ on page 4
- ‘G 133-69’ on page 4
- ‘A 399’ on page 4
- ‘Mrk 3’ on page 4
- ‘MS 0737.9+7441’ on page 4
- ‘Cl 0939+4713’ on page 4
- ‘B2 1028+31’ on page 4
- ‘B2 1128+31’ on page 4
- ‘Mrk 205’ on page 4
- ‘MS 1229.2+6430’ on page 4
- ‘HD 117555’ on page 4
- ‘A 1837’ on page 4
- ‘UZ Lib’ on page 4
- ‘PKS 2126-15’ on page 4
- ‘PKS 2135-14’ on page 4
- ‘PB 5062’ on page 4
- ‘LBQS 2212-1759’ on page 4
- ‘PHL 5200’ on page 4
- ‘IRAS 22491-1808’ on page 4
- ‘EQ Peg’ on page 4
- ‘XMSJ 001744.6+162815’ on page 14
- ‘XMSJ 001800.9+163626’ on page 14
- ‘XMSJ 001802.7+161642’ on page 14
- ‘XMSJ 001817.3+161740’ on page 14
- ‘XMSJ 001821.7+161943’ on page 14
- ‘XMSJ 001831.9+162926’ on page 14
- ‘XMSJ 001837.2+163446’ on page 14
- ‘XMSJ 001838.3+162007’ on page 14
- ‘XMSJ 001841.8+162032’ on page 14
- ‘XMSJ 001845.7+163345’ on page 14
- ‘XMSJ 001851.8+161621’ on page 14
- ‘XMSJ 001853.5+162751’ on page 14
- ‘XMSJ 001901.9+161646’ on page 14
- ‘XMSJ 001911.8+161854’ on page 14
- ‘XMSJ 001919.1+162015’ on page 14
- ‘XMSJ 001928.0+163120’ on page 14
- ‘XMSJ 010320.3-064159’ on page 14
- ‘XMSJ 010324.6-065537’ on page 14
- ‘XMSJ 010327.3-064643’ on page 14
- ‘XMSJ 010333.9-064016’ on page 14
- ‘XMSJ 010337.0-063337’ on page 14
- ‘XMSJ 010339.9-065225’ on page 14
- ‘XMSJ 010502.5-062124’ on page 14
- ‘XMSJ 010506.6-061510’ on page 14
- ‘XMSJ 021703.4-045533’ on page 14
- ‘XMSJ 021705.4-045654’ on page 14
- ‘XMSJ 021708.7-045741’ on page 14
- ‘XMSJ 021753.5-045541’ on page 14
- ‘XMSJ 021753.7-045748’ on page 14
- ‘XMSJ 021808.3-045845’ on page 15
- ‘XMSJ 021815.4-045618’ on page 15
- ‘XMSJ 021817.2-050258’ on page 15
- ‘XMSJ 021817.4-045112’ on page 15
- ‘XMSJ 021820.5-050426’ on page 15
- ‘XMSJ 021821.8-043449’ on page 15
- ‘XMSJ 021822.1-050613’ on page 15
- ‘XMSJ 021827.2-045456’ on page 15
- ‘XMSJ 021829.9-045514’ on page 15
- ‘XMSJ 021830.5-045623’ on page 15
- ‘XMSJ 021842.9-050437’ on page 15
- ‘XMSJ 021855.1-044328’ on page 15
- ‘XMSJ 021902.6-044628’ on page 15
- ‘XMSJ 021903.5-043935’ on page 15
- ‘XMSJ 021905.7-051038’ on page 15
- ‘XMSJ 021908.3-045500’ on page 15
- ‘XMSJ 021921.7-043641’ on page 15
- ‘XMSJ 021922.6-044058’ on page 15
- ‘XMSJ 021923.3-045148’ on page 15
- ‘XMSJ 021931.0-044956’ on page 15
- ‘XMSJ 021934.3-050857’ on page 15
- ‘XMSJ 021934.6-044141’ on page 15
- ‘XMSJ 021939.2-051132’ on page 15
- ‘XMSJ 021948.3-045128’ on page 15
- ‘XMSJ 022002.1-050101’ on page 15
- ‘XMSJ 022004.8-045514’ on page 15
- ‘XMSJ 022013.0-045113’ on page 15
- ‘XMSJ 022016.8-045646’ on page 15
- ‘XMSJ 025727.7+131504’ on page 15
- ‘XMSJ 025737.9+131623’ on page 15
- ‘XMSJ 025744.7+131538’ on page 15
- ‘XMSJ 025748.3+131406’ on page 15
- ‘XMSJ 025748.5+132317’ on page 15
- ‘XMSJ 025756.5+130836’ on page 15
- ‘XMSJ 025808.4+132351’ on page 15
- ‘XMSJ 025808.8+132225’ on page 15
- ‘XMSJ 025815.3+130938’ on page 15
- ‘XMSJ 025850.9+131809’ on page 15
- ‘XMSJ 025855.3+132503’ on page 15
- ‘XMSJ 025906.3+131225’ on page 15
- ‘XMSJ 061316.7+710947’ on page 15
- ‘XMSJ 061322.5+705429’ on page 15

- ‘XMSJ 074248.7+742747’ on page 16
 ‘XMSJ 074350.8+743839’ on page 16
 ‘XMSJ 074352.9+744257’ on page 16
 ‘XMSJ 074400.4+744056’ on page 16
 ‘XMSJ 074435.6+744444’ on page 16
 ‘XMSJ 074457.9+742156’ on page 16
 ‘XMSJ 074646.9+744500’ on page 16
 ‘XMSJ 074728.9+743804’ on page 16
 ‘XMSJ 083859.0+705043’ on page 16
 ‘XMSJ 084132.3+704757’ on page 16
 ‘XMSJ 084144.2+704653’ on page 16
 ‘XMSJ 084150.4+705008’ on page 16
 ‘XMSJ 084211.8+710146’ on page 16
 ‘XMSJ 084217.1+710009’ on page 16
 ‘XMSJ 084221.6+705758’ on page 16
 ‘XMSJ 084239.9+704431’ on page 16
 ‘XMSJ 084310.1+705557’ on page 16
 ‘XMSJ 084324.3+705235’ on page 16
 ‘XMSJ 084334.6+704734’ on page 16
 ‘XMSJ 094152.2+465116’ on page 16
 ‘XMSJ 094154.6+470637’ on page 16
 ‘XMSJ 094242.1+470618’ on page 16
 ‘XMSJ 094251.5+464729’ on page 16
 ‘XMSJ 094317.3+470040’ on page 16
 ‘XMSJ 094345.2+465155’ on page 16
 ‘XMSJ 094348.3+470155’ on page 16
 ‘XMSJ 102950.8+310109’ on page 16
 ‘XMSJ 103007.0+311124’ on page 16
 ‘XMSJ 103015.5+310138’ on page 16
 ‘XMSJ 103020.7+305637’ on page 16
 ‘XMSJ 103028.4+305659’ on page 16
 ‘XMSJ 103048.5+305702’ on page 17
 ‘XMSJ 103050.9+310538’ on page 17
 ‘XMSJ 103101.8+305144’ on page 17
 ‘XMSJ 103104.7+305637’ on page 17
 ‘XMSJ 103111.3+310332’ on page 17
 ‘XMSJ 103123.0+310330’ on page 17
 ‘XMSJ 103150.6+310817’ on page 17
 ‘XMSJ 103154.1+310731’ on page 17
 ‘XMSJ 103157.0+310535’ on page 17
 ‘XMSJ 113034.4+312422’ on page 17
 ‘XMSJ 113042.5+311227’ on page 17
 ‘XMSJ 113049.2+311403’ on page 17
 ‘XMSJ 113052.1+310940’ on page 17
 ‘XMSJ 113102.9+311015’ on page 17
 ‘XMSJ 113117.0+310039’ on page 17
 ‘XMSJ 113118.4+310114’ on page 17
 ‘XMSJ 113121.8+310254’ on page 17
 ‘XMSJ 113126.6+311241’ on page 17
 ‘XMSJ 122110.8+751119’ on page 17
 ‘XMSJ 122120.4+751618’ on page 17
 ‘XMSJ 122135.0+750916’ on page 17
 ‘XMSJ 122135.2+752838’ on page 17
 ‘XMSJ 122143.6+752238’ on page 17
 ‘XMSJ 122206.7+752614’ on page 17
 ‘XMSJ 122226.8+752742’ on page 17
 ‘XMSJ 122233.4+750303’ on page 17
 ‘XMSJ 122344.7+751923’ on page 17
 ‘XMSJ 122351.0+752228’ on page 17
 ‘XMSJ 122435.0+750810’ on page 17
 ‘XMSJ 122445.5+752225’ on page 18
 ‘XMSJ 123049.9+640848’ on page 18
 ‘XMSJ 123110.8+641849’ on page 18
 ‘XMSJ 123116.6+641113’ on page 18
 ‘XMSJ 123129.3+642215’ on page 18
 ‘XMSJ 123139.9+641123’ on page 18
 ‘XMSJ 123141.1+642132’ on page 18
 ‘XMSJ 123214.1+640455’ on page 18
 ‘XMSJ 123218.6+640309’ on page 18
 ‘XMSJ 123325.9+641450’ on page 18
 ‘XMSJ 132943.5+241123’ on page 18
 ‘XMSJ 132958.6+242435’ on page 18
 ‘XMSJ 133009.5+241938’ on page 18
 ‘XMSJ 133012.2+241921’ on page 18
 ‘XMSJ 133012.4+241301’ on page 18
 ‘XMSJ 133015.7+241015’ on page 18
 ‘XMSJ 133023.8+241708’ on page 18
 ‘XMSJ 133026.1+241357’ on page 18
 ‘XMSJ 133026.5+241521’ on page 18
 ‘XMSJ 133027.7+242430’ on page 18
 ‘XMSJ 133038.1+240528’ on page 18
 ‘XMSJ 133041.0+241120’ on page 18
 ‘XMSJ 133108.8+240249’ on page 18
 ‘XMSJ 133109.5+242302’ on page 18
 ‘XMSJ 133118.1+241405’ on page 18
 ‘XMSJ 133120.4+242304’ on page 18
 ‘XMSJ 133122.4+241300’ on page 18
 ‘XMSJ 133127.4+242100’ on page 18
 ‘XMSJ 140044.0-110034’ on page 18
 ‘XMSJ 140046.6-111216’ on page 18
 ‘XMSJ 140049.5-110738’ on page 18
 ‘XMSJ 140050.6-111243’ on page 18
 ‘XMSJ 140059.9-110941’ on page 18
 ‘XMSJ 140100.5-110009’ on page 18
 ‘XMSJ 140101.8-111223’ on page 18
 ‘XMSJ 140105.7-110659’ on page 18
 ‘XMSJ 140215.6-110718’ on page 18
 ‘XMSJ 140219.5-110458’ on page 18

- ‘XMSJ 212934.7-154428’ on page 19
- ‘XMSJ 212956.2-153850’ on page 19
- ‘XMSJ 213000.8-154632’ on page 19
- ‘XMSJ 213712.6-142321’ on page 19
- ‘XMSJ 213714.1-142619’ on page 19
- ‘XMSJ 213720.0-144458’ on page 19
- ‘XMSJ 213739.7-143626’ on page 19
- ‘XMSJ 213744.0-143632’ on page 19
- ‘XMSJ 213746.6-144223’ on page 19
- ‘XMSJ 213747.7-144510’ on page 19
- ‘XMSJ 213755.8-142749’ on page 19
- ‘XMSJ 213809.5-142917’ on page 19
- ‘XMSJ 213811.8-142619’ on page 19
- ‘XMSJ 213813.1-143653’ on page 19
- ‘XMSJ 213813.8-143852’ on page 19
- ‘XMSJ 213814.6-142618’ on page 19
- ‘XMSJ 213820.2-142532’ on page 19
- ‘XMSJ 213824.5-143129’ on page 19
- ‘XMSJ 213830.5-143639’ on page 19
- ‘XMSJ 220421.3-020425’ on page 19
- ‘XMSJ 220441.5-021007’ on page 19
- ‘XMSJ 220449.6-015817’ on page 19
- ‘XMSJ 220450.2-015342’ on page 19
- ‘XMSJ 220508.0-020100’ on page 19
- ‘XMSJ 220530.0-015739’ on page 19
- ‘XMSJ 221453.1-174232’ on page 19
- ‘XMSJ 221456.7-175050’ on page 19
- ‘XMSJ 221515.2-173222’ on page 19
- ‘XMSJ 221518.8-174003’ on page 19
- ‘XMSJ 221519.4-175109’ on page 19
- ‘XMSJ 221523.6-174318’ on page 19
- ‘XMSJ 221536.7-173355’ on page 19
- ‘XMSJ 221537.6-173802’ on page 19
- ‘XMSJ 221538.1-174631’ on page 19
- ‘XMSJ 221550.4-175207’ on page 19
- ‘XMSJ 221550.4-172947’ on page 20
- ‘XMSJ 221601.1-173721’ on page 20
- ‘XMSJ 221603.1-174316’ on page 20
- ‘XMSJ 221604.6-175217’ on page 20
- ‘XMSJ 221623.2-174055’ on page 20
- ‘XMSJ 221623.5-174316’ on page 20
- ‘XMSJ 221623.5-174723’ on page 20
- ‘XMSJ 222729.1-051647’ on page 20
- ‘XMSJ 222732.1-051643’ on page 20
- ‘XMSJ 222745.7-052539’ on page 20
- ‘XMSJ 222812.3-052814’ on page 20
- ‘XMSJ 222813.9-051623’ on page 20
- ‘XMSJ 222815.1-052417’ on page 20
- ‘XMSJ 222822.1-052733’ on page 20
- ‘XMSJ 225130.4-174138’ on page 20
- ‘XMSJ 225153.8-174014’ on page 20
- ‘XMSJ 225155.6-175835’ on page 20
- ‘XMSJ 225159.8-174216’ on page 20
- ‘XMSJ 225208.8-174121’ on page 20
- ‘XMSJ 225210.8-180127’ on page 20
- ‘XMSJ 225211.6-174438’ on page 20
- ‘XMSJ 225219.5-174215’ on page 20
- ‘XMSJ 225227.6-180223’ on page 20
- ‘XMSJ 225228.2-174917’ on page 20
- ‘XMSJ 233049.5+200122’ on page 20
- ‘XMSJ 233113.8+200506’ on page 20
- ‘XMSJ 233119.3+194512’ on page 20
- ‘XMSJ 233128.1+194605’ on page 20
- ‘XMSJ 233156.2+195123’ on page 20
- ‘XMSJ 233158.7+194440’ on page 21
- ‘XMSJ 233201.5+200406’ on page 21
- ‘XMSJ 233203.2+200626’ on page 21
- ‘XMSJ 233207.3+200529’ on page 21
- ‘XMSJ 233209.8+194517’ on page 21
- ‘XMSJ 233212.2+200557’ on page 21
- ‘XMSJ 233226.5+195736’ on page 21
- ‘XMSJ 233228.2+195809’ on page 21
- ‘XMSJ 233232.0+195116’ on page 21
- ‘XMSJ 233232.6+195809’ on page 21
- ‘XMSJ 001744.6+162815’ on page 22
- ‘XMSJ 001800.9+163626’ on page 22
- ‘XMSJ 001802.7+161642’ on page 22
- ‘XMSJ 001817.3+161740’ on page 22
- ‘XMSJ 001821.7+161943’ on page 22
- ‘XMSJ 001831.9+162926’ on page 22
- ‘XMSJ 001837.2+163446’ on page 22
- ‘XMSJ 001838.3+162007’ on page 22
- ‘XMSJ 001841.8+162032’ on page 22
- ‘XMSJ 001845.7+163345’ on page 22
- ‘XMSJ 001851.8+161621’ on page 22
- ‘XMSJ 001853.5+162751’ on page 22
- ‘XMSJ 001901.9+161646’ on page 22
- ‘XMSJ 001911.8+161854’ on page 22
- ‘XMSJ 001919.1+162015’ on page 22
- ‘XMSJ 001928.0+163120’ on page 22
- ‘XMSJ 010320.3-064159’ on page 22
- ‘XMSJ 010324.6-065537’ on page 22
- ‘XMSJ 010327.3-064643’ on page 22
- ‘XMSJ 010333.9-064016’ on page 22
- ‘XMSJ 010337.0-063337’ on page 22
- ‘XMSJ 010339.9-065225’ on page 22
- ‘XMSJ 010355.6-063711’ on page 22
- ‘XMSJ 010358.0-062523’ on page 22

- ‘XMSJ 021703.4-045533’ on page 22
- ‘XMSJ 021705.4-045654’ on page 22
- ‘XMSJ 021708.7-045741’ on page 22
- ‘XMSJ 021753.5-045541’ on page 22
- ‘XMSJ 021753.7-045748’ on page 22
- ‘XMSJ 021808.3-045845’ on page 23
- ‘XMSJ 021815.4-045618’ on page 23
- ‘XMSJ 021817.2-050258’ on page 23
- ‘XMSJ 021817.4-045112’ on page 23
- ‘XMSJ 021820.5-050426’ on page 23
- ‘XMSJ 021821.8-043449’ on page 23
- ‘XMSJ 021822.1-050613’ on page 23
- ‘XMSJ 021827.2-045456’ on page 23
- ‘XMSJ 021829.9-045514’ on page 23
- ‘XMSJ 021830.5-045623’ on page 23
- ‘XMSJ 021842.9-050437’ on page 23
- ‘XMSJ 021855.1-044328’ on page 23
- ‘XMSJ 021902.6-044628’ on page 23
- ‘XMSJ 021903.5-043935’ on page 23
- ‘XMSJ 021905.7-051038’ on page 23
- ‘XMSJ 021908.3-045500’ on page 23
- ‘XMSJ 021921.7-043641’ on page 23
- ‘XMSJ 021922.6-044058’ on page 23
- ‘XMSJ 021923.3-045148’ on page 23
- ‘XMSJ 021931.0-044956’ on page 23
- ‘XMSJ 021934.3-050857’ on page 23
- ‘XMSJ 021934.6-044141’ on page 23
- ‘XMSJ 021939.2-051132’ on page 23
- ‘XMSJ 021948.3-045128’ on page 23
- ‘XMSJ 022002.1-050101’ on page 23
- ‘XMSJ 022004.8-045514’ on page 23
- ‘XMSJ 022013.0-045113’ on page 23
- ‘XMSJ 022016.8-045646’ on page 23
- ‘XMSJ 025727.7+131504’ on page 23
- ‘XMSJ 025737.9+131623’ on page 23
- ‘XMSJ 025744.7+131538’ on page 23
- ‘XMSJ 025748.3+131406’ on page 23
- ‘XMSJ 025748.5+132317’ on page 23
- ‘XMSJ 025756.5+130836’ on page 23
- ‘XMSJ 025808.4+132351’ on page 23
- ‘XMSJ 025808.8+132225’ on page 23
- ‘XMSJ 025815.3+130938’ on page 23
- ‘XMSJ 025850.9+131809’ on page 23
- ‘XMSJ 025855.3+132503’ on page 23
- ‘XMSJ 025906.3+131225’ on page 23
- ‘XMSJ 061316.7+710947’ on page 23
- ‘XMSJ 061322.5+705429’ on page 23
- ‘XMSJ 061337.9+705001’ on page 23
- ‘XMSJ 061343.7+710727’ on page 23
- ‘XMSJ 074352.9+744257’ on page 24
- ‘XMSJ 074400.4+744056’ on page 24
- ‘XMSJ 074435.6+744444’ on page 24
- ‘XMSJ 074457.9+742156’ on page 24
- ‘XMSJ 074646.9+744500’ on page 24
- ‘XMSJ 074728.9+743804’ on page 24
- ‘XMSJ 083859.0+705043’ on page 24
- ‘XMSJ 084132.3+704757’ on page 24
- ‘XMSJ 084144.2+704653’ on page 24
- ‘XMSJ 084150.4+705008’ on page 24
- ‘XMSJ 084211.8+710146’ on page 24
- ‘XMSJ 084217.1+710009’ on page 24
- ‘XMSJ 084221.6+705758’ on page 24
- ‘XMSJ 084239.9+704431’ on page 24
- ‘XMSJ 084310.1+705557’ on page 24
- ‘XMSJ 084324.3+705235’ on page 24
- ‘XMSJ 084334.6+704734’ on page 24
- ‘XMSJ 094152.2+465116’ on page 24
- ‘XMSJ 094154.6+470637’ on page 24
- ‘XMSJ 094242.1+470618’ on page 24
- ‘XMSJ 094251.5+464729’ on page 24
- ‘XMSJ 094317.3+470040’ on page 24
- ‘XMSJ 094345.2+465155’ on page 24
- ‘XMSJ 094348.3+470155’ on page 24
- ‘XMSJ 102950.8+310109’ on page 24
- ‘XMSJ 103007.0+311124’ on page 24
- ‘XMSJ 103015.5+310138’ on page 24
- ‘XMSJ 103020.7+305637’ on page 24
- ‘XMSJ 103028.4+305659’ on page 24
- ‘XMSJ 103048.5+305702’ on page 25
- ‘XMSJ 103050.9+310538’ on page 25
- ‘XMSJ 103101.8+305144’ on page 25
- ‘XMSJ 103104.7+305637’ on page 25
- ‘XMSJ 103111.3+310332’ on page 25
- ‘XMSJ 103123.0+310330’ on page 25
- ‘XMSJ 103150.6+310817’ on page 25
- ‘XMSJ 103154.1+310731’ on page 25
- ‘XMSJ 103157.0+310535’ on page 25
- ‘XMSJ 113034.4+312422’ on page 25
- ‘XMSJ 113042.5+311227’ on page 25
- ‘XMSJ 113049.2+311403’ on page 25
- ‘XMSJ 113052.1+310940’ on page 25
- ‘XMSJ 113102.9+311015’ on page 25
- ‘XMSJ 113117.0+310039’ on page 25
- ‘XMSJ 113118.4+310114’ on page 25
- ‘XMSJ 113121.8+310254’ on page 25
- ‘XMSJ 113126.6+311241’ on page 25
- ‘XMSJ 113129.3+310945’ on page 25
- ‘XMSJ 113138.2+311230’ on page 25

- ‘XMSJ 122135.0+750916’ on page 25
- ‘XMSJ 122135.2+752838’ on page 25
- ‘XMSJ 122143.6+752238’ on page 25
- ‘XMSJ 122206.7+752614’ on page 25
- ‘XMSJ 122226.8+752742’ on page 25
- ‘XMSJ 122233.4+750303’ on page 25
- ‘XMSJ 122344.7+751923’ on page 25
- ‘XMSJ 122351.0+752228’ on page 25
- ‘XMSJ 122435.0+750810’ on page 25
- ‘XMSJ 122445.5+752225’ on page 26
- ‘XMSJ 123049.9+640848’ on page 26
- ‘XMSJ 123110.8+641849’ on page 26
- ‘XMSJ 123116.6+641113’ on page 26
- ‘XMSJ 123129.3+642215’ on page 26
- ‘XMSJ 123139.9+641123’ on page 26
- ‘XMSJ 123141.1+642132’ on page 26
- ‘XMSJ 123214.1+640455’ on page 26
- ‘XMSJ 123218.6+640309’ on page 26
- ‘XMSJ 123325.9+641450’ on page 26
- ‘XMSJ 132943.5+241123’ on page 26
- ‘XMSJ 132958.6+242435’ on page 26
- ‘XMSJ 133009.5+241938’ on page 26
- ‘XMSJ 133012.2+241921’ on page 26
- ‘XMSJ 133012.4+241301’ on page 26
- ‘XMSJ 133015.7+241015’ on page 26
- ‘XMSJ 133023.8+241708’ on page 26
- ‘XMSJ 133026.1+241357’ on page 26
- ‘XMSJ 133026.5+241521’ on page 26
- ‘XMSJ 133027.7+242430’ on page 26
- ‘XMSJ 133038.1+240528’ on page 26
- ‘XMSJ 133041.0+241120’ on page 26
- ‘XMSJ 133108.8+240249’ on page 26
- ‘XMSJ 133109.5+242302’ on page 26
- ‘XMSJ 133118.1+241405’ on page 26
- ‘XMSJ 133120.4+242304’ on page 26
- ‘XMSJ 133122.4+241300’ on page 26
- ‘XMSJ 133127.4+242100’ on page 26
- ‘XMSJ 140044.0-110034’ on page 26
- ‘XMSJ 140046.6-111216’ on page 26
- ‘XMSJ 140049.5-110738’ on page 26
- ‘XMSJ 140050.6-111243’ on page 26
- ‘XMSJ 140059.9-110941’ on page 26
- ‘XMSJ 140100.5-110009’ on page 26
- ‘XMSJ 140101.8-111223’ on page 26
- ‘XMSJ 140105.7-110659’ on page 26
- ‘XMSJ 140215.6-110718’ on page 26
- ‘XMSJ 140219.5-110458’ on page 26
- ‘XMSJ 153134.0-083610’ on page 26
- ‘XMSJ 153142.0-082109’ on page 26
- ‘XMSJ 213000.8-154632’ on page 27
- ‘XMSJ 213712.6-142321’ on page 27
- ‘XMSJ 213714.1-142619’ on page 27
- ‘XMSJ 213720.0-144458’ on page 27
- ‘XMSJ 213739.7-143626’ on page 27
- ‘XMSJ 213744.0-143632’ on page 27
- ‘XMSJ 213746.6-144223’ on page 27
- ‘XMSJ 213747.7-144510’ on page 27
- ‘XMSJ 213755.8-142749’ on page 27
- ‘XMSJ 213809.5-142917’ on page 27
- ‘XMSJ 213811.8-142619’ on page 27
- ‘XMSJ 213813.1-143653’ on page 27
- ‘XMSJ 213813.8-143852’ on page 27
- ‘XMSJ 213814.6-142618’ on page 27
- ‘XMSJ 213820.2-142532’ on page 27
- ‘XMSJ 213824.5-143129’ on page 27
- ‘XMSJ 213830.5-143639’ on page 27
- ‘XMSJ 220421.3-020425’ on page 27
- ‘XMSJ 220441.5-021007’ on page 27
- ‘XMSJ 220449.6-015817’ on page 27
- ‘XMSJ 220450.2-015342’ on page 27
- ‘XMSJ 220508.0-020100’ on page 27
- ‘XMSJ 220530.0-015739’ on page 27
- ‘XMSJ 221453.1-174232’ on page 27
- ‘XMSJ 221456.7-175050’ on page 27
- ‘XMSJ 221515.2-173222’ on page 27
- ‘XMSJ 221518.8-174003’ on page 27
- ‘XMSJ 221519.4-175109’ on page 27
- ‘XMSJ 221523.6-174318’ on page 27
- ‘XMSJ 221536.7-173355’ on page 27
- ‘XMSJ 221537.6-173802’ on page 27
- ‘XMSJ 221538.1-174631’ on page 27
- ‘XMSJ 221550.4-175207’ on page 27
- ‘XMSJ 221550.4-172947’ on page 28
- ‘XMSJ 221601.1-173721’ on page 28
- ‘XMSJ 221603.1-174316’ on page 28
- ‘XMSJ 221604.6-175217’ on page 28
- ‘XMSJ 221623.2-174055’ on page 28
- ‘XMSJ 221623.5-174316’ on page 28
- ‘XMSJ 221623.5-174723’ on page 28
- ‘XMSJ 222729.1-051647’ on page 28
- ‘XMSJ 222732.1-051643’ on page 28
- ‘XMSJ 222745.7-052539’ on page 28
- ‘XMSJ 222812.3-052814’ on page 28
- ‘XMSJ 222813.9-051623’ on page 28
- ‘XMSJ 222815.1-052417’ on page 28
- ‘XMSJ 222822.1-052733’ on page 28
- ‘XMSJ 222823.7-051306’ on page 28
- ‘XMSJ 222826.5-051820’ on page 28

- ‘XMSJ 225155.6-175835’ on page 28
- ‘XMSJ 225159.8-174216’ on page 28
- ‘XMSJ 225208.8-174121’ on page 28
- ‘XMSJ 225210.8-180127’ on page 28
- ‘XMSJ 225211.6-174438’ on page 28
- ‘XMSJ 225219.5-174215’ on page 28
- ‘XMSJ 225227.6-180223’ on page 28
- ‘XMSJ 225228.2-174917’ on page 28
- ‘XMSJ 233049.5+200122’ on page 28
- ‘XMSJ 233113.8+200506’ on page 28
- ‘XMSJ 233119.3+194512’ on page 28
- ‘XMSJ 233128.1+194605’ on page 28
- ‘XMSJ 233156.2+195123’ on page 28
- ‘XMSJ 233158.7+194440’ on page 29
- ‘XMSJ 233201.5+200406’ on page 29
- ‘XMSJ 233203.2+200626’ on page 29
- ‘XMSJ 233207.3+200529’ on page 29
- ‘XMSJ 233209.8+194517’ on page 29
- ‘XMSJ 233212.2+200557’ on page 29
- ‘XMSJ 233226.5+195736’ on page 29
- ‘XMSJ 233228.2+195809’ on page 29
- ‘XMSJ 233232.0+195116’ on page 29
- ‘XMSJ 233232.6+195809’ on page 29